NTNU – Trondheim
Norwegian University of
Science and Technology

Effect of free stream turbulence on wind turbine performance

Kristine Mikkelsen

EPT-M-2013-84

MASTER THESIS

for

student Kristine Mikkelsen

Spring 2013

Effect of free stream turbulence on wind turbine performance

Effekt av fristrømsturbulens på vindturbinens ytelser

Background and objective

When the aerodynamic characteristics of a wind turbine is to be mapped, it is common to assume that the incoming flow field is uniform and free from turbulence. This is important because it is then possible to derive analytical expressions for theories that predict the performance and it also reduces some uncertainties in experimental verifications of the results.

In real life operations the turbines operate in the atmospheric boundary layer, which typically has turbulence intensities of the order of 10 to 15%. It is to be expected that this affects both the performance characteristics of the turbine, as well as the wake development downstream. In this case the performance of turbines further downstream are also likely to be affected, so for a wind park the effect of turbulence may be significant.

The department has been studying extensively the performance of a model turbine in uniform, low turbulence flow. We would now like to study the effects of free stream turbulence.

The following tasks are to be considered:

1) The student should study the literature in order to find what the expected effect of free stream turbulence on wind turbine performance and wake development is.
2) The student should study classical grid turbulence theory to be able to devise a method of generating a suitable level of turbulence in the wind tunnel.
3) An experimental study of the performance and wake development downstream of our model turbine should be performed both at close to zero turbulence level, as well as at a typical turbulence level. The results should be compared and possible differences investigated.

Within 14 days of receiving the written text on the master thesis, the candidate shall submit a research plan for his project to the department.

When the thesis is evaluated, emphasis is put on processing of the results, and that they are presented in tabular and/or graphic form in a clear manner, and that they are analyzed carefully.

The thesis should be formulated as a research report with summary both in English and Norwegian, conclusion, literature references, table of contents etc. During the preparation of the text, the candidate should make an effort to produce a well-structured and easily readable report. In order to ease the evaluation of the thesis, it is important that the cross-references are correct. In the making of the report, strong emphasis should be placed on both a thorough discussion of the results and an orderly presentation.

The candidate is requested to initiate and keep close contact with his/her academic supervisor(s) throughout the working period. The candidate must follow the rules and regulations of NTNU as well as passive directions given by the Department of Energy and Process Engineering.
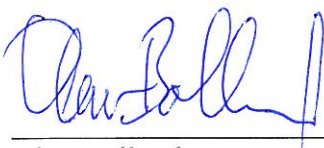
Risk assessment of the candidate's work shall be carried out according to the department's procedures. The risk assessment must be documented and included as part of the final report. Events related to the candidate's work adversely affecting the health, safety or security, must be documented and included as part of the final report. If the documentation on risk assessment represents a large number of pages, the full version is to be submitted electronically to the supervisor and an excerpt is included in the report.

Pursuant to "Regulations concerning the supplementary provisions to the technology study program/Master of Science" at NTNU §20, the Department reserves the permission to utilize all the results and data for teaching and research purposes as well as in future publications.
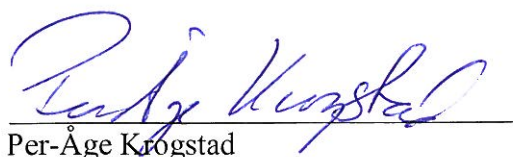
The final report is to be submitted digitally in DAIM. An executive summary of the thesis including title, student's name, supervisor's name, year, department name, and NTNU's logo and name, shall be submitted to the department as a separate pdf file. Based on an agreement with the supervisor, the final report and other material and documents may be given to the supervisor in digital format.

☒ Work to be done in lab (Water power lab, Fluids engineering lab, Thermal engineering lab)
☐ Field work

Department of Energy and Process Engineering, 14. January 2013

Olav Bolland
Department Head

Per-Åge Krøgstad
Academic Supervisor

Preface

This Master Thesis has been conducted at the Department of Energy and Process Engineering at the Norwegian University of Science and Technology, and is the conclusion of five years at the study program "Energy and Environmental Engineering".

First of all I want to thank my supervisor Per-Åge Krogstad for the guidance throughout the process of completing this Master Thesis. His insight and experience have been most helpful, and I am truly grateful for his guidance.

I also want to thank Pål Egil Eriksen, a ph.d candidate at the Department, for teaching me how to use a hot wire and for all the help during the lab experiments. Finally, I want to thank Arnt Egil Kolstad for the help with installing and moving equipment in the wind tunnel.

Kristine Mikkelsen
Trondheim, 5.juni 2013

Abstract

In this Master Thesis the effect of free stream turbulence has been investigated on a model wind turbine's performance characteristics and the wake development downstream. The experiment took place in the recirculating wind tunnel in the Fluid Mechanics building at NTNU, and the model wind turbine that was used had a diameter of 0,9 meter. A turbulence-generating grid with a mesh size of 0,24 meters produced a turbulence intensity of 5,5 % in front of the wind turbine, which corresponds to atmospheric turbulence levels offshore. The experimental results with free stream turbulence were compared to the results without free stream turbulence. A reference wind speed of approximately 10 m/s were used in all the experiments.

The wind turbine is operating most efficiently at $TSR \approx 6$, and the peak power coefficient without free stream turbulence was $C_P = 0,461$, while it was $C_P = 0,45$ with free stream turbulence. Hence, the power coefficient seemed to be slightly reduced with increased levels of turbulence, except at low tip speed ratios where the effect of stall dominated. The free stream turbulence has two opposite effects on the power extraction of the wind turbine, and this may be the reason why the peak power coefficient was only reduced by 2,4 % with free stream turbulence, which was lower than expected. Increased levels of turbulence increase the drag on the turbine blades, which reduces the power extraction. Simultaneously, the power extraction is proportional to the square of the relative velocity at the blades, which increases with higher levels of turbulence.

Wake measurements were performed with a hot wire which measured the velocities and the normal stresses in the streamwise direction. The measurements were done across the wake at the distances 1, 3 and 5 rotor diameters downstream of the wind turbine. The thrust coefficients at $TSR \approx 6$ are almost identical both with and without free stream turbulence, and the velocity profiles just behind the rotor are therefore also almost identical. However, the effect of the free stream turbulence is clearly seen downstream in the wake, where velocity gradients, inhomogeneities and the kinetic energy in the tip vortices are smoothed and more spread out with free stream turbulence. This is due to increased turbulent diffusion, which is increasing the radial transport of momentum in the wake. The velocity profiles in the wake hence become flatter and broader, and the wake recovers faster with higher levels of turbulence. Even though the power extraction is slightly reduced with free stream turbulence, it seems like the effect on the recovery of the wake is larger, which will lead to higher power extraction and lower fatigue loads on a downwind turbine. Increased levels of ambient turbulence will therefore probably increase the total power output in a wind farm.

The length scale of the turbulence produced from the grid was approximately 0,2 meters, which was about 5-6 times smaller than desired compared to a wind turbine in the free atmosphere. The effect of the free stream turbulence on the performance characteristics and wake development of the model wind turbine might therefore be smaller than for a wind turbine in an open environment, and further studies should therefore be performed to investigate this effect.

Sammendrag

I denne masteroppgaven har effekten av fristrømsturbulens på en vindturbins ytelse og vakeutvikling blitt undersøkt. Eksperimentene har blitt gjennomført i den resirkulerende vindtunnelen i Strømningsteknisk bygg på NTNU, og vindturbinen som ble brukt hadde en diameter på 0,9 meter. Et turbulens-genererende grid med en maskestørrelse på 0,24 meter ble brukt for å produsere en turbulensintensitet på 5,5 % foran vindturbinen, noe som tilsvarer atmosfæriske turbulensnivåer offshore. De eksperimentelle resultatene med fristrømsturbulens ble sammenlignet med resultatene uten fristrømsturbulens. En referansehastighet på omtrent 10 m/s ble brukt i alle eksperimentene.

Vindturbinen kjører mest effektivt ved $TSR \approx 6$, og den maksimale effektkoeffisienten uten fristrømsturbulens var $C_P = 0,461$, mens den var $C_P = 0,45$ med fristrømsturbulens. Effektkoeffisienten ser dermed ut til å reduseres noe med høyere turbulensnivåer, bortsett fra ved lave spisshastighetsrater hvor effekten av "stall" er dominerende. Fristrømsturbulensen har to motsatte effekter på effektuttaket til vindturbinen, og dette kan være grunnen til at den maksimale effektkoeffisienten kun ble redusert med 2,4 % med fristrømsturbulens, noe som var lavere enn forventet. Høyere turbulensnivåer øker motstanden på turbinbladene, noe som reduserer effektuttaket. Samtidig er effektuttaket proporsjonalt med kvadratet av den relative hastigheten ved bladene, som øker med økt turbulens.

Vakemålingene ble utført med en hot wire som målte hastighetene og normalspenningene i strømretningen. Målingene ble utført på tvers av vaken ved avstandene 1, 3 og 5 rotordiametere nedstrøms fra vindturbinen. Motkraftskoeffisientene ved $TSR \approx 6$ er nesten identiske både med og uten fristrømsturbulens, og hastighetsprofilene rett bak rotoren er derfor også nesten identiske. I midlertidig, effekten av fristrømsturbulens er lett å se lengre nedstrøms, hvor hastighetsgradienter, inhomogeniteter og den kinetiske energien i vingespissvirvlene er jevnet ut og mer spredd ut med fristrømsturbulens. Denne effekten skjer på grunn av økt turbulent diffusjon, som øker den radielle transporten av bevegelsesmengde i vaken. Hastighetsprofilene i vaken blir dermed flatere og bredere, og vaken gjenvinnes raskere ved økt turbulens. Selv om effektuttaket er noe redusert med fristrømsturbulens, ser det ut som effekten på gjenvinningen av vaken er større, som vil føre til høyere effektuttak for en nedstrøms vindturbin. Økte atmosfæriske turbulensnivåer vil derfor sannsynligvis øke det totale effektuttaket i en vindpark.

Lengdeskalaen til turbulensen som blir produsert fra gridet i vindtunnelen var omtrent 5-6 ganger mindre enn ønsket, sammenlignet med en vindturbin i den frie atmosfæren. Effekten av fristrømsturbulens på vindturbinens ytelse og vakeutvikling kan derfor være lavere enn for en vindturbin i åpne omgivelser. Videre studier burde derfor bli gjennomført for å undersøke effekten av den turbulente lengdeskalaen på en vindturbins ytelser og vakeutviklingen nedstrøms.

Contents

List of Figures

List of Tables

Nomenclature

Symbol	Definition
a	Axial induction factor
a'	Angular induction factor
A	Area
c	chord length of wind turbine blade
C_p	Pressure coefficient
C_P	Power coefficient
C_T	Thrust coefficient
C_l	Lift coefficient
C_d	Drag coefficient
D	Wind turbine diameter or drag force
E	Energy
f	Frequency of fluctuating wind
f(u)	Probability density function
F_u	Flatness factor
k	Turbulent kinetic energy
K	Overheating factor for hot wire resistance
l	Span of airfoil
L	Lift force
$^x L_u$	Integral length scale
m	Mass
$\dot{m}$	Mass flow rate
M	Mesh spacing of grid
pdf	Probability density function
p_∞	Free stream static pressure
P	Power
P	Production of turbulent kinetic energy
Q	Torque
r	Local radius on wind turbine blade
R	Radius of wind turbine rotor
R_w	Hot wire resistance
Re	Reynolds number
S_u	Skewness factor
T	Thrust force
T_u	Turbulence intensity
TSR	Tip Speed ratio
u	Instantaneous wind speed
u'	Fluctuating part of instantaneous wind velocity
$\overline{u}$	Mean wind speed
$\overline{u'u'}$	Normal stress
U	Mean velocity
U_{ref}	Reference/free stream wind speed
U_∞	Reference/free stream wind speed
U_{rel}	Relative wind velocity
z	Height above ground/sea level
z_0	Surface roughness

Greek symbols

Symbol	Definition
α	Angle of attack
α	Overheating factor for hot wire material
δ	Height of atmospheric boundary layer
ϵ	Dissipation of turbulent kinetic energy
λ	Tip speed ratio, also called TSR
ρ	Density
μ	Dynamic viscosity
ν	Kinematic viscosity
ω	Rotational speed of wake
Ω	Rotational speed of wind turbine
θ_p	Section pitch angle
$\phi = \theta_p + \alpha$	Angle of relative wind
Φ_{uu}	Normalized power spectrum
σ	Solidity
σ_u	Standard deviation of wind velocity
$\theta_T = \theta_p - \theta_{p0}$	Section twist angle
θ_{p0}	Pitch angle at blade tip

Chapter 1

Introduction

According to the International Energy Agency's *World Energy Outlook 2012* [4], "No more than one-third of proven reserves of fossil fuels can be consumed prior to 2050 if the world is to achieve the 2 ℃ goal, unless carbon capture and storage (CCS) technology is widely deployed". At the same time, they claim that the world's energy demand will increase by more that one third until 2035, based on their central scenario. Developing more renewable energy and increasing the energy efficiency will therefore be key factors to decrease the effect of global warming and meet the future's energy demand.

The energy potential of offshore wind is enormous. According to the Global Wind Energy Council [5], it could meet Europe's energy demand seven times over. Although offshore wind is often the most talked about part of the wind sector, today it represents less than 2 % of global installed wind power capacity. The major reason for this is the challenge for offshore wind to continue to bring down costs. Studies to increase the efficiency of wind farms are therefore important to increase the cost efficiency. The effect of ambient turbulence on wind turbine performance is one important aspect to be investigated.

When the aerodynamic characteristics of a wind turbine is to be mapped, it is common to assume that the incoming flow field is uniform and free from turbulence. But in real life wind turbines operates in the atmospheric boundary layer, where turbulence is present in the incoming flow. This is expected to influence the performance of the wind turbine, as well as the wake development downstream. The effect of turbulence in a wind park may therefore be significant. The objective of this Master Thesis is therefore to perform an experimental study on the effect of free stream turbulence on wind turbine performance and wake development. A model wind turbine in a wind tunnel will be used for the experiments, and a turbulence-generating grid will produce free stream turbulence. The power coefficient and thrust coefficient curves with an incoming flow field both with and without free stream turbulence will be compared, in addition to the wake profiles at the distances 1, 3 and 5 rotor diameters downstream of the wind turbine. It will be assumed that the model wind turbine in the wind tunnel is comparable to a full-scale wind turbine in offshore environments.

Some studies have been done on the effect of atmospheric turbulence intensity on wind farm efficiency. According to Barthelmie et al. (2007) [13] the power losses due to turbine

wakes in large offshore wind farms are about 10-20 % of the total power output. They also showed that the turbulence intensity offshore at hub-heights above 50 meters is typically less than 6 %, which is lower than over land surfaces. In another study conducted by Barthelmie et al. (2012) [11], the ambient turbulent intensity's influence on the wind farm efficiency at Horns Rev Wind Farm in Denmark was investigated, for the wind speed range 7-8 m/s. They found that the wind farm efficiency increases almost linearly with the ambient turbulence intensity level for this wind speed range. This was confirmed in a study by Turk & Emeis (2010) [14], who found that power output in a wind farm, and also loads on rotor blades, increase with increasing levels of turbulence intensity.

A numerical study performed by Wu & Porté-Agel (2012) [16] showed that when the turbulence intensity level of the incoming flow is higher, the turbine-induced wake (velocity deficit) recovers faster, and the locations of the maximum turbulence intensity and turbulent stress are closer to the turbine. Several studies ([11], [30], [31]) have shown that increased turbulence is improving the wake recovery due to enhanced mixing of the air in turbulent flows. According to Medici & Alfredsson (2006) the ambient turbulence level has no effect on the wake deficit in the near wake, up to a distance of 2 rotor diameters downstream. However, the effect of free stream turbulence, i.e. of the enhanced radial transport of momentum due to velocity fluctuations, was clearly seen at a distance of 3 diameters downstream of the wind tunnel. The effect of free stream turbulence on a wind turbine's performance and wake development is to be further investigated in this Master Thesis.

Chapter 2

Aerodynamics of wind turbines

2.1 One-dimensional momentum theory

Wind turbine power production depends on the interactions between the rotor and the wind. Even though the wind can be considered as a combination of the mean wind and turbulent fluctuations, the major aspects of wind turbine performance are determined by the aerodynamic forces generated by the mean wind. Wind shear, off-axis wind, rotor rotation, turbulence and dynamic effects are forces that lead to fatigue loads and peak loads, but first the aerodynamics of steady state operations have to be understood.

Today most wind turbines are horizontal axis wind turbines (HAWT), consisting of blades mounted perpendicular to a horizontal axis. The turbines transform the kinetic energy in the wind into electrical energy. The kinetic energy of an air mass m moving at a velocity U can be expressed as:

$$E = \frac{1}{2}mU^2 \tag{2.1}$$

The mass flow rate of air with density ρ, passing through the rotor cross-sectional area A, is $\dot{m} = \rho U A$. The power available in the air stream is then:

$$P = \frac{1}{2}\rho U^3 A \quad (W) \tag{2.2}$$

A classical analytical approach on horizontal axis wind turbines can be used to determine the power from an ideal wind turbine using momentum theory. Betz (1926) was one of the original developers of the classical analysis of wind turbines, and he developed a simple model which is based on linear momentum theory [1]. By looking at an individual wind turbine, this model assumes a control volume around a stream tube that passes through the wind turbine rotor. The turbine itself is represented by an "actuator disc", which creates a discontinuity of pressure in the air flowing through it.

The assumptions used in this analysis are:

- Homogeneous, incompressible, steady state flow

- No frictional drag

- Uniform thrust

- Non-rotating wake

- Infinite number of blades

- The static pressure far upstream and far downstream is equal to the ambient static pressure

For steady-state flow, the mass flow rate is defined as $\dot{m} = (\rho U A)_1 = (\rho U A)_4$, using the numbered locations as illustrated in figure 2.1. U_1 is assumed to be equal to the free stream velocity U. By applying conservation of linear momentum, one can find the thrust, which is the force of the wind on the wind turbine:

$$T = U_1(\rho A U)_1 - U_4(\rho A U)_4 = \dot{m}(U_1 - U_4) \tag{2.3}$$

where ρ is the air density, U is the air velocity and A is the cross-sectional area at their respective locations. The thrust can also be expressed as the net sum of the forces on each side of the actuator disc:

$$T = A_2(p_2 - p_3) \tag{2.4}$$

The flow is assumed to be stationary, frictionless, incompressible and with no external forces acting on it. Therefore the Bernoulli function can be used in two control volumes upstream and downstream of the actuator disc, respectively:

$$p_1 + \frac{1}{2}\rho U_1^2 = p_2 + \frac{1}{2}\rho U_2^2 \tag{2.5}$$

$$p_3 + \frac{1}{2}\rho U_3^2 = p_4 + \frac{1}{2}\rho U_4^2 \tag{2.6}$$

Assuming the far upstream and far downstream pressures are equal to the free stream static pressure ($p_1 = p_4 = p_\infty$), and that the velocity across the disc remains the same ($U_2 = U_3$), the thrust can be expressed as:

$$T = \frac{1}{2}\rho A_2(U_1^2 - U_4^2) \tag{2.7}$$

Using $\dot{m} = (\rho U A)_2$ and equating equation 2.3 and 2.7, the wind velocity at the rotor plane can be expressed as:

$$U_2 = \frac{U_1 + U_4}{2} \tag{2.8}$$

Defining an axial induction factor:

$$a = \frac{U_1 - U_2}{U_1} \tag{2.9}$$

The velocities can then be expressed as:

$$U_2 = U_1(1 - a) \tag{2.10}$$

$$U_4 = U_1(1 - 2a) \tag{2.11}$$

The power output, P, is equal to the thrust T times U_2:

$$P = \frac{1}{2}\rho A_2(U_1^2 - U_4^2)U_2 \tag{2.12}$$

or

$$P = \frac{1}{2}\rho AU^3 4a(1 - a)^2 \tag{2.13}$$

U is here the free stream velocity and A is the rotor area A_2. Similarly, the thrust can also be expressed in terms of the axial induction factor:

$$T = \frac{1}{2}\rho AU^2 4a(1 - a) \tag{2.14}$$

The theory derived in this section is only applicable for an axial induction factor of $a < \frac{1}{2}$. $a = \frac{1}{2}$ corresponds to a velocity of zero behind the rotor, which is physically impossible. The fluid flow needs some kinetic energy to be transported away from behind the rotor.

The power coefficient, C_P, for the wind turbine rotor performance, represents the fraction of the power in the wind that is extracted by the rotor:

$$C_P = \frac{P_{extracted}}{P_{available}} = \frac{P}{\frac{1}{2}\rho AU^3} \tag{2.15}$$

where U is the free stream velocity. From equation 2.13, the expression for the power coefficient becomes:

$$C_P = 4a(1 - a)^2 \tag{2.16}$$

The thrust on a wind turbine can also be characterized by a non-dimensional thrust coefficient:

$$C_T = \frac{T}{\frac{1}{2}\rho AU^2} = \frac{Thrust force}{Dynamic force} = 4a(1 - a) \tag{2.17}$$

Figure 2.2 shows the power coefficient for a wind turbine versus the axial induction factor a. Setting $\frac{dC_P}{da} = 0$ one can calculate the maximum $C_{P,max} = \frac{16}{27} = 0.5926$, which corresponds to an axial induction factor of $a = \frac{1}{3}$. This maximum limit is called Betz limit. More details about the calculations can be found in the book Wind Energy Explained [1].
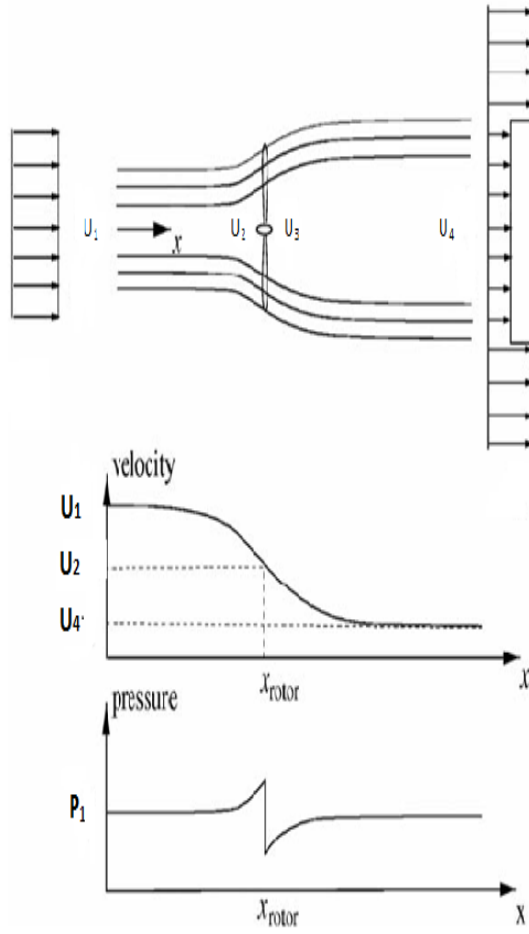
Figure 2.1: Illustration of the streamlines across the rotor, the axial velocity and the pressure [6].
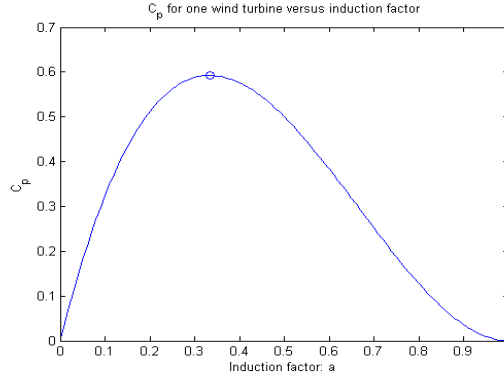
Figure 2.2: Power coefficient for one wind turbine versus axial induction factor a.

2.2   Wake rotation

Betz limit, $C_{P,max} = \frac{16}{27}$, is the maximum theoretically possible rotor power coefficient. But in practice there are effects that decrease the maximum achievable power, amongst them:

- Rotation of wake behind the rotor

- Finite number of blades and associated tip losses

- Non-zero aerodynamic drag

In addition to the linear momentum theory, the rotor also generates angular momentum in the wake behind the rotor, which results in less energy extraction by the rotor than without wake rotation. The flow behind the rotor will rotate in the opposite direction to the rotor, as a reaction to the torque exerted by the flow on the rotor.

In addition to the axial induction factor a, an angular induction factor a' is also defined:

$$a' = \frac{\omega}{2\Omega} \tag{2.18}$$

where Ω is the angular velocity of the wind turbine rotor, and ω is the angular velocity imparted to the flow stream.

The tip speed ratio, λ, of a wind turbine is an important characteristic, which is defined as:

$$\lambda = \frac{\Omega R}{U} \tag{2.19}$$

where U is the free stream velocity and R is the rotor radius. The tip speed ratio is often abbreviated to TSR.

In the following analysis, a stream tube with radius r and thickness dr is used, such that the pressure, the wake rotation and the induction factors become dependent on r. r is the local radius from the centre of the rotor to the point on the blade that is considered. Across a flow disc the angular velocity of the air increases from Ω to $\Omega + \omega$, while the

7

axial component remains constant. Using the energy equation on a control volume that moves with the blade, the pressure difference across the blade can be expressed as [1]:

$$p_2 - p_3 = \rho(\Omega + \frac{1}{2}\omega)\omega r^2 \tag{2.20}$$

Using the above equations, the thrust on an annular element dT can be expressed as:

$$dT = 4a'(1+a')\frac{1}{2}\rho\Omega^2 r^2 2\pi r dr = 4a(1-a)\frac{1}{2}\rho U^2 2\pi r dr \tag{2.21}$$

By applying conservation of angular momentum, one can derive an expression for the torque. The torque, Q, exerted on the rotor, is equal to the change of angular momentum of the wake. For an incremental annular area element the torque is:

$$dQ = d\dot{m}(\omega r)r = 4a'(1-a)\frac{1}{2}\rho U\Omega r^2 2\pi r dr \tag{2.22}$$

The expressions for the power at each element, and the power coefficient are shown in equations 2.23 and 2.24 respectively.

$$dP = \Omega dQ \tag{2.23}$$

$$C_P = \frac{dP}{\frac{1}{2}\rho AU^3} = \frac{8}{\lambda^2}\int_0^\lambda a'(1-a)\lambda_r^3 d\lambda_r \tag{2.24}$$

where λ_r is the local tip speed ratio. For more detailed calculations, see [1].

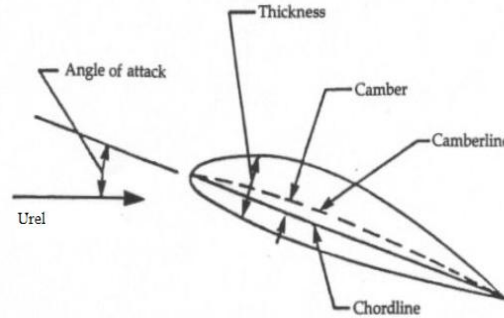## 2.3 Airfoils and blade aerodynamics

Figure 2.3: Airfoil nomenclature.

The cross-sections of wind turbine blades have the shape of airfoils, which have special geometric shapes that generate mechanical forces due to the relative motion of the airfoil

and the surrounding fluid. An airfoil and some of it's nomenclature is shown in figure 2.3. The angle of attack, α, is defined as the angle between the relative wind and the chord line. The chord line, c, is the strait line between the leading and trailing edge, while the camberline is the line that goes halfway between the upper and lower surface. The camber is therefore defined as the thickest distance between the chord line and the camberline.

The relative wind velocity U_{rel} is the relative velocity between the axial velocity U and the rotational velocity $r\Omega$ at the local intermediate radius r, defined by the equation:

$$U_{rel}^2 = U^2 + (r\Omega)^2 \tag{2.25}$$

A velocity triangle is shown in figure 2.4, where ϕ is the angle of the relative wind, which is the sum of the section pitch angle and angle of attack ($\phi = \theta_p + \alpha$). The section pitch angle θ_p is the angle between the chord line and the plane of rotation. The leading edge radius, the trailing edge angle, the maximum thickness, the thickness distribution of the profile and the mean camber line are geometric parameters of the airfoil that have an effect on it's aerodynamic performance.
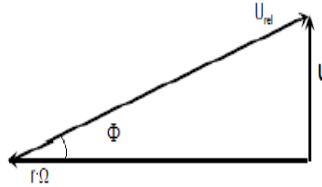
Figure 2.4: Illustration of the relative wind velocity.

2.3.1 Lift and drag

The air that flows over an airfoil produces pressure and friction forces on the surface. The suction side of the surface is the convex and upper side of the blade, where the flow velocity increases and the average pressure decreases. The concave side on the lower surface of the blade therefore becomes the pressure side of the airfoil. In addition, there is viscous friction that will slow the air flow next to the surface. These pressure and viscous forces are often resolved into a lift force, a drag force and a pitching moment acting along the chord with a distance of $\frac{c}{4}$ from the leading edge [1]. The lift and drag forces are illustrated in figure 2.5. The lift force is defined to be perpendicular to the airflow, and is therefore a consequence of the unequal pressure distribution on the lower and upper side of the airfoil. The drag force is defined parallel to the incoming airflow, and is due to both viscous friction at the surface and unequal pressure distribution on airfoil surfaces. The pitching moment is defined about an axis perpendicular to the airfoil cross-section.

An important non-dimensional parameter to characterize fluid flow is the Reynolds number:

$$Re = \frac{UL}{\nu} = \frac{\rho UL}{\mu} \tag{2.26}$$

9
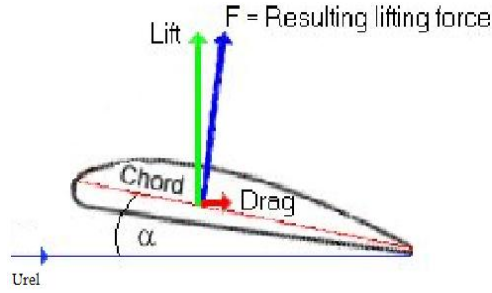
Figure 2.5: Illustration of the lift and drag forces on an airfoil.

where L is the characteristic length, U is the incoming wind velocity, ν is the kinematic viscosity and μ is the dynamic viscosity. The characteristic length for a turbine blade is typically the chord length c. The Reynolds number is the ratio between inertia forces to viscous forces, and for a flat plate the critical local Reynolds number for transition between laminar and turbulent flow is $5 \cdot 10^5$ [2]. For airfoils, the Reynolds number is commonly in the turbulent range. The lift and drag forces are often expressed as non-dimensional coefficients, which are dependent on the Reynolds number. For two-dimensional airfoils, it is assumed that they have an infinite span, hence no end effects. The two-dimensional lift and drag coefficients are defined in equation 2.27 and 2.28, respectively:

$$C_l = \frac{\frac{L}{l}}{\frac{1}{2}\rho U^2 c} \tag{2.27}$$

$$C_d = \frac{\frac{D}{l}}{\frac{1}{2}\rho U^2 c} \tag{2.28}$$

where l is the airfoil span.

The pressure coefficient is also a dimensionless coefficient that is important for the analysis and design of wind turbines:

$$C_p = \frac{p - p_\infty}{\frac{1}{2}\rho U^2} \tag{2.29}$$

2.3.2 Flow over an airfoil and stalled airfoils

As explained in section 2.3.1, the forces and moment acting on an airfoil are generated by the pressure variation on the airfoil surface and the friction between the air and the airfoil. When the air flow accelerates around the rounded leading edge, the pressure drops and results in a negative pressure gradient. Approaching the trailing edge, the air flow decelerates and results in a positive pressure gradient. Given the airfoil design and

10

the angle of attack, if the air speeds up more over the upper surface than over the lower surface of the airfoil, then there is a net lift force.

The drag on the airfoil creates a boundary layer surrounding the wind turbine blade, where the velocity increases from zero at the airfoil surface to that of the friction-free flow outside the boundary layer. The thickness of this boundary layer may vary from a millimetre to tens of centimetres [1]. The flow in the boundary layer can be either laminar, which is smooth and steady flow, or turbulent, with three dimensional vortices. A laminar boundary layer is thinner and has lower frictional forces than a turbulent boundary layer, which is thicker and has higher frictional forces. At the leading edge the flow is laminar, but usually the flow transforms into chaotic, turbulent flow downstream on the airfoil.

The flow in the boundary layer surrounding a wind turbine blade is accelerated or decelerated by the pressure gradient, and the flow is also slowed by surface friction. This pressure gradient can either be a favourable pressure gradient, which is positive in the direction of the flow, or an adverse pressure gradient, which is against the flow. An adverse pressure gradient, in addition to surface friction, can stop the airflow in the boundary layer or reverse it's direction. The airflow is then separating from the airfoil, and cause a condition called stall. This will make the boundary layer on the airfoil grow, and it will alter the effective geometry of the airfoil. Stalled airfoils result in reduced performance due to a drop of the lift force and an increase of the drag force. The larger the angle of attack is, the closer the separation point moves towards the leading edge. The separation point tends to move backwards and forwards, causing dynamic forces acting on the airfoil. Turbulent boundary layers are less sensitive to adverse pressure gradients than laminar boundary layers. An illustration of a stalled airfoil and an attached airfoil is shown in figure 2.6.

It is important to distinguish between the effects of the turbulence in the atmosphere and the turbulent flow in the boundary layer of an airfoil. The length scales of the atmospheric turbulence are much larger than that of the boundary layer, and the atmospheric turbulence does not affect the airfoil boundary layer directly [1]. It may affect it indirectly through changing angles of attack, which will change the pressure distribution and flow pattern over the blade surface. If the level of the atmospheric turbulence increases, the flow in the boundary layer of the blade will transform into a turbulent boundary layer faster.
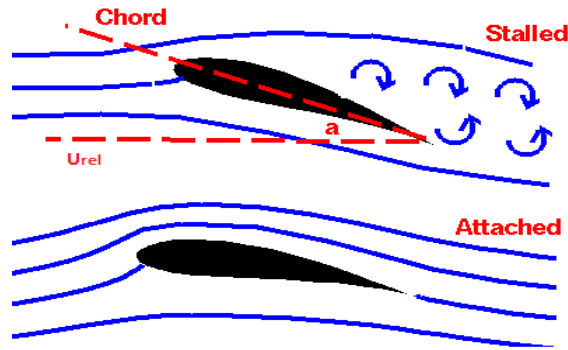
Figure 2.6: Illustration of stalled and attached flow over an airfoil.

2.4 Wake development

In a wind farm, the energy that is extracted by the upwind wind turbines results in lower wind speeds and increased turbulence for the wind turbines downwind. These wake effects are decreasing the energy production and increase fatigue loads on downwind turbines. The energy losses due to wake effects in wind farms are called array losses, and these losses are functions of the wind turbine spacing, the wind turbine operating characteristics, the number of turbines, the turbulence intensity, etc. The energy loss will be replenished by exchange of kinetic energy with the surroundings, after a certain distance. The wake's length and width depend on the rotor size and the turbine's power production.

When regarding the wake of a wind turbine, a distinction can be made between the near wake and the far wake. According to Ainslie (1988) [32] there exists a complex near wake region behind the rotor which depends on the geometry of the rotor and typically extends over about 2-4 diameters downstream. This region is dominated by axial and radial pressure gradients caused by the extraction of energy at the rotor disc. The maximum velocity deficit is typically found 1 to 2 diameters downstream, beyond which fluid mixing takes over from the pressure gradients effects as the dominant process in the flow, and the velocity begins to recover. The far wake is the region beyond the near wake and the shape of the rotor in this region is less important. The far wake is interesting for wind farm performance investigations when turbines are standing in the wake of other upstream turbines.

The one-dimensional momentum theory described in section 2.1 assumes that the control volume surrounding the wake is separated from the free flow outside the wake. In reality a shear layer between the wake and the free stream is created due to the velocity differences. The shear layer thickens while moving downstream, and the place where it meets the axis of the wake is the end of the near wake region [31]. In this shear layer turbulent eddies are formed, and the ambient shear layer leads to higher turbulence intensities at the upper part of the wake. The higher the thrust is on the rotor, the lower the wake velocity is and the higher the shear. The turbulence in the wake mixes the lower velocities in the wake with the higher velocities in the free wind stream, and this process is called entrainment. This transfer of momentum leads to expansion of the wake, and the rate at which this

occurs depends on the ambient turbulence level. An illustration of the transition between the near and far wake is shown in figure 2.7. In the far wake, the wake is fully developed and the decrease of the velocity deficit depends on the turbulence levels of the wake. While the wake in the near wake is highly non-uniform, the wake in the far wake region is approximately axisymmetric, self-similar and Gaussian [31].

In addition to this shear-generated turbulence, the turbine itself creates turbulence as a result of the tip vortices shed by the blades and the general disturbance to the flow caused by the blades, nacelle and tower. In the atmospheric boundary layer there is also ambient turbulence present, which increases the recovery of the wake.
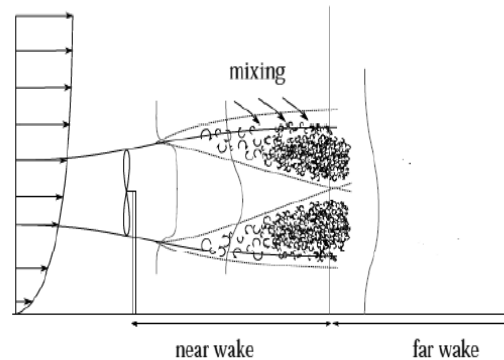
Figure 2.7: Illustration of near and far wake downstream of a turbine [31](modified).

13

2.4.1   Tip loss and tip vortex

The rotation of the wake creates a tangential velocity distribution, and the airflow in the wake rotates in the opposite direction of the turbine. At each turbine blade a bound vortex with strength Γ is generating the lift through Kutta-Joukowski law: $L = \rho U \Gamma$ [31]. The pressure difference between the lower and upper surface at the tip of the blade leads to the formation of a tip vortex. This is reducing lift, and hence power production near the tip. There is one vortex generated from the tip of each blade, which follows a helical path with rotation opposite to the rotor. Two pictures of tip vortices from a wind turbine in steady, uniform and parallel flow conditions are shown in figure 2.8 and 2.9. There is also formed a root vortex from the root of the blades, and the tower and nacelle will disturb the flow around the centreline of the rotor.
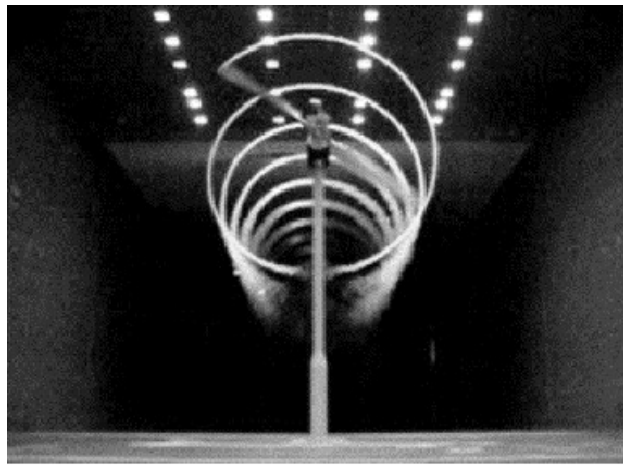
Figure 2.8: Picture of tip vortex with view from the front of the wind turbine.
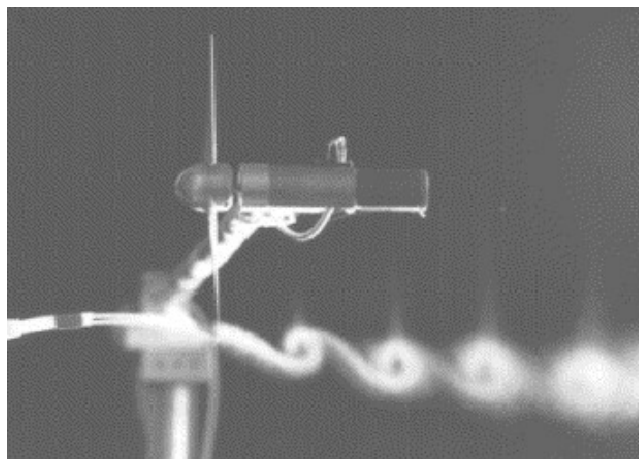
Figure 2.9: Picture of tip vortex with view from the side of the wind turbine.

Chapter 3

Turbulence

3.1 The atmospheric boundary layer

The original source of the energy contained in the earth's wind resource is the sun. Uneven heating of the earth by solar radiation causes pressure differences across the earth's surface, and hence produces global winds. In addition to these pressure forces, the Coriolis force caused by the rotation of the earth, inertial forces due to large-scale circular motion and frictional forces at the earth's surfaces are influencing the characteristics of the wind motion [1].

The earth's surface retards the air flow and produces a horizontal drag force on the moving air. This effect is diffused by turbulent mixing throughout a region which is called the atmospheric boundary layer. The height of this boundary layer is denoted δ and can vary from a few hundred meters to several kilometres, depending on the wind intensity, the roughness of the terrain and the angle of latitude [8]. Due to the no-slip condition of viscous fluids like air, one expects the horizontal wind speed to be zero at the earth's surface and that it increases with height in the atmospheric boundary layer. The maximum wind speed is often called gradient velocity in atmospheric flows and free stream velocity in laboratory flows. The variation of wind speed with elevation is called the vertical wind shear, and this is a very important design parameter in wind energy engineering. It determines the productivity of a wind turbine at a certain hight and it also influences the lifetime of a turbine rotor blade.

3.1.1 Mean velocity profiles

The vertical wind profiles can be found by putting up masts with anemometers and measure the wind speed over time. Since this is costly and time consuming, it is more common to use mathematical models that estimate the vertical wind shear. There are two mathematical models that are widely used to model the vertical profile of wind speed over regions of homogeneous, flat terrain: the log-law and the power law. The equation

known as the logarithmic wind profile is defined as:

$$U(z) = \frac{U^*}{k} ln(\frac{z}{z_0})$$

(3.1)

where z is the elevation above the ground, z_0 is the surface roughness length and k=0,4 is von Karman's constant [1]. $U^* = \sqrt{\frac{\tau_0}{\rho}}$ is defined as the friction velocity, where ρ is the density of the air and τ_0 is the surface value of the shear stress. The roughness length z_0 describes the roughness of the ground or terrain where the wind is blowing. Values for the roughness length of different terrain are found in various articles and books, and an example from Wind Energy Handbook [9] is shown in figure 3.1.

Type of terrain	Roughness length z_0(m)
Cities, forests	0.7
Suburbs, wooded countryside	0.3
Villages, countryside with trees and hedges	0.1
Open farmland, few trees and buildings	0.03
Flat grassy plains	0.01
Flat desert, rough sea	0.001

Figure 3.1: Typical surface roughness lengths. From Wind Energy Handbook [9].

The basic form of the power law is:

$$\frac{U(z)}{U_{ref}} = \left(\frac{z}{z_{ref}}\right)^\alpha$$

(3.2)

where U(z) is the wind speed at height z, $U(z_{ref})$ is the reference wind speed at the reference height z_{ref} and α is the power law exponent. α depends on the surface roughness and the atmospheric stability. According to Counihan (1975) [17], α is an indication of the amount of turbulence present in the atmosphere. The power law is widely used due to it's simplicity, and it seems to give a better fit to most of the data over a greater height range and for higher wind conditions, compared to the log-law. The power law is therefore often used in wind power assessment.

3.1.2 Atmospheric stability

The stability of the atmospheric boundary layer is determined after it's tendency to resist vertical motion or to suppress existing turbulence. It is usually classified as stable, neutrally stable or unstable and is governed by the vertical temperature distribution of the atmosphere. Unstable stratification occurs when there is a lot of surface heating, causing warm air near the surface to rise [9]. The air then cools adiabatically, but if the cooling is not enough to bring the air into thermal equilibrium with it's surroundings, it will continue to rise and produce large convection cells. This results in a thick boundary

layer with large-scale turbulent eddies, and there is a lot of vertical mixing and transfer of momentum. Stable stratification occurs when the adiabatic cooling effect causes the rising air to become colder than it's surroundings, which results in suppression of vertical motion. Then the turbulence is dominated by friction with the ground, and the wind shear is high in stable conditions. In the neutral atmosphere, the air that rises is in thermal equilibrium with it's surroundings. A strictly neutral atmosphere is uncommon, but when it is cloudy and during periods with strong winds, near-neutral conditions can occur.

The stability of the atmosphere therefore influences the turbulence intensity, and the atmosphere tends towards lower levels of turbulence for more stable conditions. This is shown in figure 3.2 [12]. Stable conditions are associated with lower levels of turbulence intensity, and even though stable conditions can persist at high wind speeds, higher wind speeds tend to force conditions towards neutral. Though atmospheric stability represents levels of atmospheric turbulence, this relationship is highly wind speed dependent. Atmospheric turbulence differs from turbulence generated in a laboratory or in pipe flow. In the atmosphere, convective turbulence coexists with mechanical turbulence.
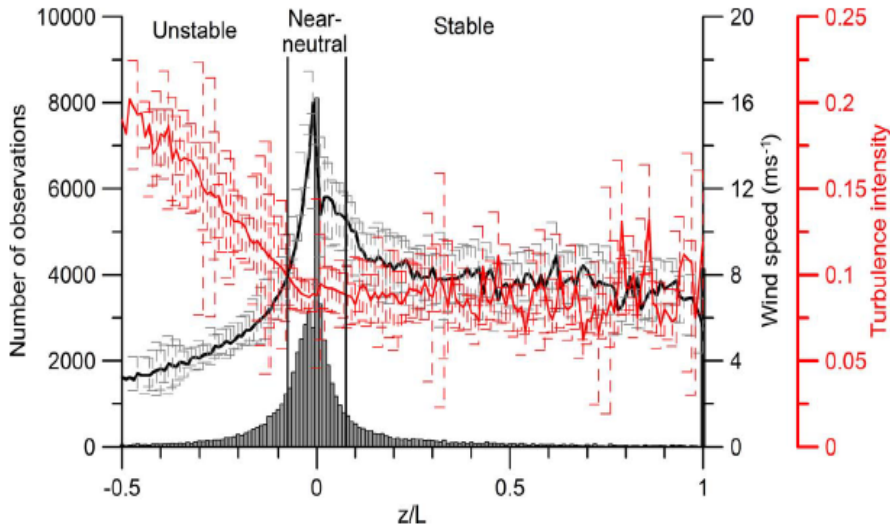
Figure 3.2: Relationship between turbulence intensity and wind speed with atmospheric stability at 70 m height for all wind speeds and directions at Horns Rev [12].

According to Barthelmie et al.(2012)([11], [12]), the total wind farm efficiency tends to increase with increasing turbulence intensity and decrease towards more stable atmospheric conditions. They also found that the turbulence intensity offshore at hub-heights above 50 meters is typically less than 6 %, and that it is lowest in the wind speed range between 8-12 m/s. Hence, the turbulence intensity can be higher than 6 % for wind speeds lower or higher than this range. The wake is found to be wider and deeper in very stable conditions due to decreased turbulent mixing. The maximum power deficit in the centre of the wake is also slightly less in near-neutral and unstable conditions than in stable conditions. The power deficit is also shown to decrease almost linearly with turbulence intensity [11]. Hence, increased atmospheric mixing promotes wake recovery

17

and decreases power losses. However, it is the wind speed that has the largest effect on the total wind farm efficiency.

3.2 Turbulence

Turbulence in the wind is caused by dissipation of the wind's kinetic energy into thermal energy through the creation and destruction of progressively smaller eddies [1]. It is generated from friction with the earth's surface and thermal effects, which can cause air masses to be moved vertically as a result of temperature variations. Turbulent fluctuations always have a three-dimensional spatial distribution, and visualisations of turbulent flow reveal rotational flow structures, which are the so-called eddies. Turbulence is a complex process, and in order to derive the Navier-Stokes equations including turbulence, one has to take into account temperature, density, pressure and humidity as well as the motion of the air itself in three dimensions. The problem is that small changes in initial conditions or boundary conditions can lead to large differences in the flow after a short amount of time, hence turbulence is chaotic and very difficult to predict. Therefore it is more common to develop descriptions of turbulence in terms of statistical methods.

Turbulence may be characterized by a relatively constant short-term mean, with fluctuations about the mean. The instantaneous wind speed in the three dimensions u, v and w can be defined as, respectively:

$$u = U + u' = \overline{u} + u' \tag{3.3}$$

$$v = V + v' = \overline{v} + v' \tag{3.4}$$

$$w = W + w' = \overline{w} + w' \tag{3.5}$$

where U,V and W, or $\overline{u}$, $\overline{v}$ and $\overline{w}$, are the short-term mean wind speeds for the longitudinal, lateral and vertical directions respectively. The short-term mean wind speed refers to mean wind speed averaged over some (short) time period. u', v' and w' are the respective superimposed fluctuating wind of zero mean. Since the velocity at a fixed point in turbulent or fluctuating flow is a random variable in time, it is normal to use statistics to describe the flow. The probability that the wind speed has a particular value can be described in terms of a probability density function. From experience, the wind speed is more likely to be close to it's mean value than far from it, and the probability density function that best describes the type of behaviour for turbulence is the Gaussian distribution [1]:

$$f(u) = \frac{1}{\sigma_u \sqrt{2\pi}} exp[-\frac{(u - U)^2}{2\sigma_u^2}] \tag{3.6}$$

Quantities called moments of the distribution are defined by the relation:

$$b_n = \int\limits_{-\infty}^{\infty} u^n f(u) du \tag{3.7}$$

18

where n=0,1,2,... is the order of the moment [28]. n=1 corresponds to the average velocity $\overline{u}$:

$$b_1 = \overline{u} = \frac{1}{T} \int_{t_0}^{t_0+T} u \, dt = \int_{-\infty}^{\infty} u f(u) \, du \tag{3.8}$$

One usually works with moments about the mean, or central moments, and these quantities are defined as:

$$B_n = \int_{-\infty}^{\infty} (u - \overline{u})^n f(u) \, du \tag{3.9}$$

It is obvious that $B_1 = 0$ from this equation, and the second moment is then:

$$B_2 = Var(u) = \overline{(u')^2} = \sigma_u^2 \tag{3.10}$$

The second order moment is hence the variance of u(t). The square-root of the variance is the standard deviation:

$$\sigma_u = \sqrt{Var(u)} = \overline{(u')^2}^{\frac{1}{2}} \tag{3.11}$$

The standard deviation is also referred to as the root mean square of u, and is a quantity which serves as a measure of the width, or the spread, of the distribution.

The skewness and flatness factors are two quantities which are useful in turbulence studies. The skewness factor is the third moment non-dimensionalized with respect to the second central moment:

$$S_u = \frac{B_3}{B_2^{(3/2)}} = \frac{\overline{(u')^3}}{[\overline{(u')^2}]^{(3/2)}} \tag{3.12}$$

The skewness factor is a measure of the symmetry, or lack of symmetry, about the mean value. If the distribution of the probability density function f(u) is symmetric about the mean, then S=0. The skewness factor is negative if f(u) is leaned to the right of the mean, with a longer and fatter tail on the left. If it is positive, f(u) is leaned to the left of the mean, and the right tail is longer and fatter. An illustration of the effect of the skewness factor is shown in figure 3.3.

The flatness factor, also called kurtosis, is a measure of whether the data is peaked or flat relative to the normal distribution. It is defined as:

$$F_u = \frac{B_4}{B_2^2} = \frac{\overline{(u')^4}}{[\overline{(u')^2}]^2} \tag{3.13}$$

For the Gaussian, or normal, distribution, the flatness factor is F=3 and the skewness factor is S=0. If the flatness factor is higher than 3, the peak of f(u) will be more distinct and the tails fatter. If F is lower than 3, f(u) has a lower and wider peak around the mean and thinner tails. An illustration of the effect of the flatness factor is shown in figure 3.4.
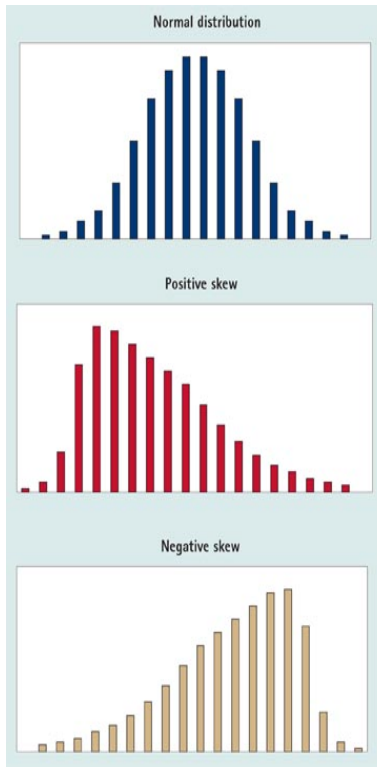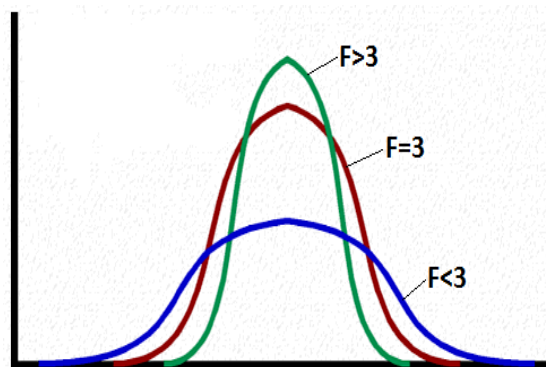
Figure 3.3: Illustration of skewness factor.

Figure 3.4: Illustration of flatness factor.

3.2.1 Turbulence intensity

Turbulence intensity in the streamwise direction is defined as:

$$T_u = \frac{\sigma_u}{U} \tag{3.14}$$

where σ_u is the standard deviation of wind speed variations about the mean wind speed U [1]. If N_s is the number of samples, the standard deviation is given by:

$$\sigma_u = \sqrt{\frac{1}{N_s - 1} \sum_{i=1}^{N_s} (u_i - U)^2} \tag{3.15}$$

The turbulence intensity depends on the roughness of the earth's surface, the height above the ground, topological features and the thermal behaviour of the atmosphere.

Figure 3.5 shows the turbulence intensity's dependency on wind speed measured from the offshore measurement platform FIN01 which is located 45 km off the coast north of the island of Borkum in the German Bight [14]. The figure shows that the turbulence intensity is highest at low wind speeds, and then decreases rapidly until about 12 m/s. When the wind speed increases above 12 m/s, the turbulence intensity increases approximately linearly with wind speed. For low wind speeds it is the thermally generated turbulence that dominates, while above about 12 m/s the mechanically generated turbulence dominates, where higher waves and hence surface roughness leads to higher turbulence intensities. This means that the turbulence intensity is lowest in the wind speed range between approximately 7-12 m/s, which is the range where the thrust coefficient is highest. In this range the turbulence intensity is about 5 % at a hub-height of 90 meter, which is in accordance with Barthelmie et al.(2012) [11].
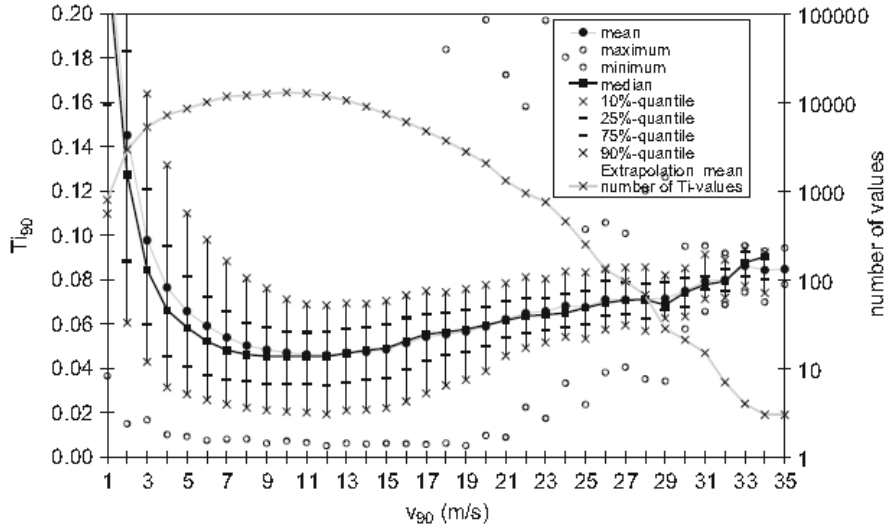

Figure 3.5: Turbulence intensity depending on wind speed 90 meters above sea level.

3.2.2 Integral length scale

Autocorrelation is the cross-correlation of a signal with itself, hence it is the similarity between observations as a function of the time separation between them. The normalized autocorrelation function $R(r\delta t)$ for a time series u'(t) relates the fluctuating part of the velocity at time t to the corresponding value at the time t+r, where r is the time lag. The function is given by:

$$R(r\delta t) = \frac{1}{\sigma_u^2(N_s - r)} \sum_{i=1}^{N_s-r} u_i u_{i+r} \tag{3.16}$$

This function has a maximum value of 1 at zero time lag, and then decreases to zero as the time lag r increases [1]. In a wind tunnel the autocorrelation function will fluctuate around 0 due to small changes in the wind velocity. An example of an autocorrelation function is shown in figure 3.6.
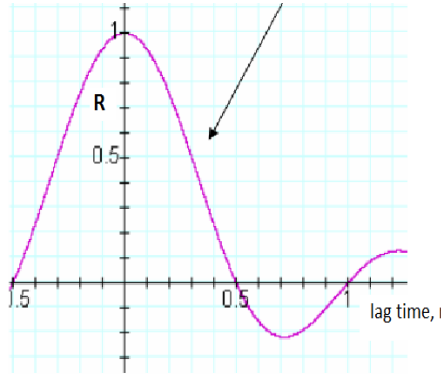
Figure 3.6: Autocorrelation function

The integral time scale T_u is found by integrating the autocorrelation function from zero lag to the first zero crossing:

$$T_u = \int_{r=0}^{r=r_{cross}} R(r\delta t)dr \tag{3.17}$$

The integral length scale ^xL_u is the average size of the eddies in the streamwise direction, and it indicates the scales of eddies containing the major part of the kinetic energy [27]. At a given height it can be calculated by multiplying the integral time scale with the mean streamwise velocity:

$$^xL_u = T_u U \tag{3.18}$$

The integral length scale in the atmospheric boundary layer decreases with increasing roughness and increases with height. ESDU recommends the following relationship to estimate the integral length scale [27].

$$^xL_u = 25\frac{z^{0,35}}{z_0^{0,063}} \tag{3.19}$$

where z is the height above the surface and z_0 is the surface roughness. According to Counihan (1975) [17],the surface roughness for the sea surface is approximately 0,001 m, though z_0 for the sea surface has been found to vary between 0,0001-0,04 m from different sources. z_0 will vary with wind speed, wave height and distance from the coast.

3.2.3 Power spectral density function

The fluctuations in the wind can be thought of as resulting from a composite of sinusoidally varying winds superimposed on the mean steady wind. These will have a variety of amplitudes, frequencies and phases, and the function that characterizes turbulence as a function of frequency is known as the spectral density function [1]. The amplitudes are characterized by their mean square values, and the function for the relation between the amplitude and the frequency originates from electrical power applications. The power spectral density function S(f) describes how the power of a time series is distributed with frequency. The average power in the turbulence within a range of frequencies can be found by integrating S(f) between two frequencies. The integral over all frequencies is equal to the total variance:

$$\sigma_u^2 = \int\limits_0^\infty S(f)df = \overline{u'^2} \tag{3.20}$$

The normalized power spectrum is:

$$\Phi_{uu}(f) = \frac{S(f)}{\sigma_u^2} \tag{3.21}$$

By plotting Φ_{uu} versus f, the total area under the curve equals 1. The area under the curve between two frequencies is hence the fraction of the variance contained between these two frequencies. An alternative is to plot $f\Phi_{uu}$ versus ln(f). The area under the curve is still equal to one, but this curve is more readable than the previous.

Power spectral densities are often used in dynamic analyses, and a number of power spectral density functions are used as models in wind energy engineering. A suitable model which is similar to one that von Karman developed for the longitudinal component of turbulence in wind tunnels is given by equation 3.22.

$$f\Phi_{uu} = \frac{4X}{(1 + 70,8X^2)^{\frac{5}{6}}}, \quad X = \frac{fL_{Karman}}{U} \tag{3.22}$$

where f is the frequency, U is the mean wind speed and L_{Karman} is the integral length scale ^xL_u at a given height. The von Karman spectrum has been shown to represent wind tunnel turbulence well [27].

3.2.4 Turbulent kinetic energy and the energy cascade

The turbulent kinetic energy can be quantified by the mean of the turbulent normal stresses:

$$k = \frac{1}{2}(\overline{u'u'} + \overline{v'v'} + \overline{w'w'}) \tag{3.23}$$

From classical theory, the energy cascade is the phenomenon that kinetic energy enters the turbulence at the largest scales of motion, and then the energy is transferred to smaller and smaller scales until the energy is dissipated by viscous action [3]. A fully turbulent flow at a high Reynolds number is considered, with characteristic velocity U and length scale L, which gives a Reynolds number of $Re = \frac{UL}{\nu}$. The largest eddies are characterized by the length scale l_0, which is comparable to the flow scale L, while the smaller eddies have length scales l. The largest eddies are unstable and break up, transferring their energy to smaller eddies. This energy transfer continues until the eddy Reynolds number $Re(l) = \frac{u(l)l}{\nu}$ is sufficiently small that the eddy motion is stable.

The equation for the evolution of turbulent kinetic energy is defined as:

$$\frac{Dk}{Dt} + \nabla \cdot T' = P - \epsilon \tag{3.24}$$

where $\nabla \cdot T'$ is the turbulent transport or turbulent diffusion, P is the production of turbulent kinetic energy (the source) and ϵ is the dissipation of turbulent kinetic energy (the sink). The diffusion term is responsible for the efficient mixing in turbulent flows, and is determined by the velocity gradients in the flow field:

$$\nabla \cdot T' = \frac{\partial \overline{ku_i}}{\partial x_j} \tag{3.25}$$

Classical theory by Kolmogorov defines length scales (η), velocity scales (u_η) and timescales (τ_η) for the very smallest, dissipative eddies. This theory states that for the small eddies, all high Reynolds number turbulent velocity fields are statistically identical when they are scaled by the Kolmogorov scales:

$$\eta = (\frac{\nu^3}{\epsilon})^{\frac{1}{4}} \tag{3.26}$$

$$u_\eta = (\epsilon\nu)^{\frac{1}{4}} \tag{3.27}$$

$$\tau_\eta = (\frac{\nu}{\epsilon})^{\frac{1}{2}} \tag{3.28}$$

For very high Reynolds numbers, the energy cascade is often divided into three regions; The energy-containing range, the inertial subrange and the dissipation range. The bulk of the energy is contained in the larger eddies with length scales in the order of l_0, therefore this range is called the energy-containing range. The dissipation range is for the smallest eddies with length scales in the order of η, where viscous effects are dominating. For very high Reynolds numbers there are length scales in between these two extrema, $l_0 \gg l \gg \eta$, and this range is called the inertial subrange because the Reynolds number is still so high that inertial effects dominate.

$E(\kappa)$ is defined as the energy spectrum function, where $\kappa = \frac{2\pi}{l}$ is the wavenumber for the corresponding length scale l [3]. The energy contained in the wavenumber range (κ_a, κ_b)

is:

$$k = \int\limits_{\kappa_a}^{\kappa_b} E(\kappa)d\kappa \tag{3.29}$$

The total turbulent kinetic energy for isotropic turbulence (grid turbulence is reasonably isotropic [3]) can therefore be expressed as:

$$k = \frac{1}{2}(\overline{u'u'} + \overline{v'v'} + \overline{w'w'}) = \int\limits_{0}^{\infty} E(\kappa)d\kappa \tag{3.30}$$

The contribution to the dissipation rate ϵ from motions in the wavenumber range (κ_a, κ_b) is:

$$\epsilon = \int\limits_{\kappa_a}^{\kappa_b} 2\nu\kappa^2 E(\kappa)d\kappa \tag{3.31}$$

More details on the energy spectrum function and turbulent flows can be found in the book "Turbulent Flows" by Pope [3].

3.2.5 Homogeneous shear flow

The definition of homogeneous turbulence is that the fluctuating components of the velocity and the pressure are statistically homogeneous. This means that all statistics are invariant under a shift in position [3]. If the field is also invariant under rotation and reflection of the coordinate system, then it is statistically isotropic.

In homogeneous flow the transport of kinetic energy is absent, and equation 3.24 simplifies to:

$$\frac{\partial k}{\partial t} = P - \epsilon \tag{3.32}$$

From experimental and simulation studies, an important conclusion is that after a development time, homogeneous shear flow becomes self-similar. The term self-similarity means that for a given geometry, any measured statistical quantity measured at different facilities and Reynolds numbers will collapse into a single universal profile if properly scaled. Homogeneous shear flow can be reasonably well approximated in wind tunnel experiments [3].

3.2.6 Grid turbulence

In the absence of mean velocity gradients, homogeneous turbulence decays because there is no production (P=0) [3]. An approximation to decaying homogeneous turbulence can be achieved if a uniform stream passes through a grid in a wind tunnel experiment. In the laboratory frame the flow is statistically stationary, and in the center of the flow, statistics vary only in the streamwise direction. The larger scales of the turbulence are expected to be self-similar when scaled with u and l, and the smaller scales to be self-similar when scale with Kolmogorov microscales ν and η. In a frame which is moving with the mean velocity U, the turbulence is homogeneous and it evolves with time.

The normal stresses and the turbulent kinetic energy decay as power laws in decaying homogeneous turbulence. One can express the turbulent intensity as:

$$\frac{\overline{u'u'}}{U^2} = T_u^2 = A(\frac{x - x_0}{M})^{-n} \tag{3.33}$$

where A is a constant, M is the mesh spacing of the grid, and n is the decay exponent. x_0 is the point at a distance $nl_0 A^{-1}\frac{U}{u_0}$ upstream of the point where the turbulence first becomes fully developed [19]. So one does not know in advance where x_0 should be, first experiments have to be performed and analysed. However, x_0 will be the same for geometrically similar grids. According to Krogstad & Davidsen (2009) [19], the minimum decay exponent in strictly homogeneous turbulence, where A=constant, is $n = \frac{6}{5}$. However, in grid turbulence, A may decline slowly in the streamwise direction. Classical theory by Kolmogorov states that the integral scales u and l satisfies $u^2 l^5 \approx constant$, while theory by Saffman states that $u^2 l^3 \approx constant$. Experiments on grid turbulence in a wind tunnel conducted by Krogstad & Davidsen (2009) showed that once the turbulence is fully developed, $u^2 l^3 \approx constant$ and the decay exponent becomes $n = 1,13 \pm 0,02$ due to the slow decline in A. They therefore concluded that turbulence behind a grid is of the Saffman type.

The initial development of the flow depends strongly on the initial conditions. According to Kistler & Vrebalovich (1966) [26], the constant A in equation 3.33 is directly related to the pressure drop across the grid. A connection between the pressure drop across the grid and the solidity of the grid is shown in figure 3.7, where the solidity is defined as the solid area of grid divided by the total area.
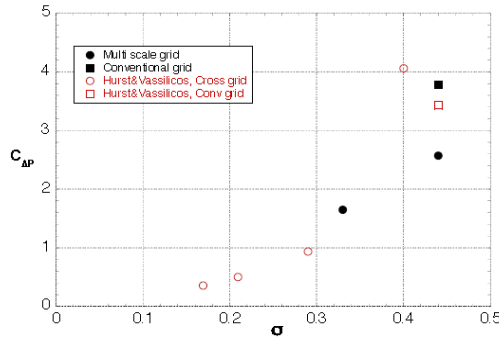

Figure 3.7: Pressure drop versus solidity for different grids [20].

Chapter 4

Experimental setup and procedures

4.1 The wind tunnel

The experiment was conducted in a recirculating wind tunnel in the Fluid Mechanics building at the Norwegian University of Science and Technology. The tunnel test section is 2,7 meters wide, 1,8 meters high and 12,2 meters long. An electric fan is generating the flow, and the wind speed is increased by increasing the rotational speed of the fan. The wind tunnel has a contraction area upwind of the test section, and a sketch is shown in figure 4.1.
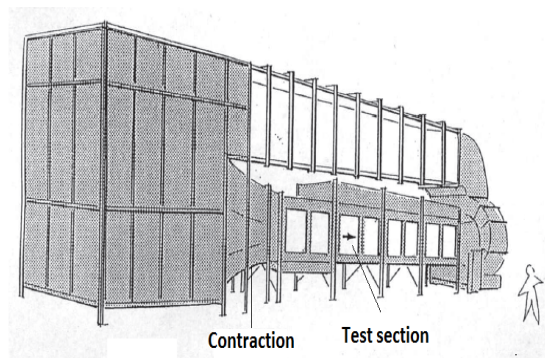
Figure 4.1: Sketch of the wind tunnel. [27]

4.1.1 Wind speed measurements

The reference wind speed was measured with a pressure transducer to find the pressure difference over the contraction. The Bernoulli equation and the continuity equation was then used to calculate the velocity. To find the real reference wind speed, a pitot static-probe was placed in an empty tunnel where the centre of the rotor was supposed to be. The velocity measurements from the pitot static-probe were used to find the relationship between the wind speed calculated from the contraction pressure difference and the real

reference wind speed: $U_{ref} = C \cdot V_2$, were C is the correction factor and V_2 is the velocity calculated from the contraction pressure difference. This resulted in the correction factors $C = \frac{1}{0,984}$ without the grid in the tunnel and $C = \frac{1}{1,1538}$ with the grid in the tunnel. A reference wind speed of $U_{ref} = 10$ m/s was used in all the experiments. The calibration curves for the pressure transducers and the velocity calculations are found in appendix A.3.

4.1.2   The turbulence-generating grid

In this Master Thesis the main focus is to compare the wind turbine's performance and the wake development downstream with and without free stream turbulence. Therefore a grid was placed at the entrance of the wind tunnel test section to generate free stream turbulence whenever this was to be investigated. The grid had square holes of 19,2 cm and a mesh size of M=24 cm. The solidity of the grid was $\sigma = 0,33$, and the drag coefficient across the grid was approximately $C_D \approx 2$. The grid covered the whole area of the entrance of the wind tunnel test section, and therefore had a total area of 2,7 m × 1,8 m. A sketch of a section of the grid is shown in figure 4.2. According to Krogstad & Davidsen [19], $\frac{x_0}{M} \approx 5,9\,m$ for a geometrical similar grid, see equation 3.33. With M=0,24 meters, the turbulence generated from the grid is therefore expected to be more or less homogeneous in front of the wind turbine.

As will be discussed later in this report, the turbulence length scale generated from this grid is smaller than expected in the free atmosphere. There were done some calculations prior to the lab experiments whether or not to make a grid with larger mesh size, to generate larger turbulent length scales. However, the dimensions of the wind tunnel were limiting, and the mesh size couldn't be increased as much as necessary. Therefore the conclusion was to keep the original grid, because the difference of increasing the mesh size a little bit would probably not make that much of a difference.

The grid was mounted at the entrance of the wind tunnel to generate free stream turbulence. When measurements were taken without free stream turbulence, the grid was disconnected at the top and then laid down on the wind tunnel floor. When measurements further out in this report are referred to as without grid, without grid turbulence or without free stream turbulence, it means that the grid was laying on the floor at the entrance of the wind tunnel test section. The grid laying on the floor will create a boundary layer which grows downstream in the wind tunnel. The thickness of this boundary layer is unknown and it may have an effect on the experimental results. This effect has been neglected in this report, and the incoming flow was assumed to be uniform and with a turbulence level close to zero when the grid was laying on the floor. This may be a source of error in the experimental results without grid turbulence, and this will be discussed later in this report.
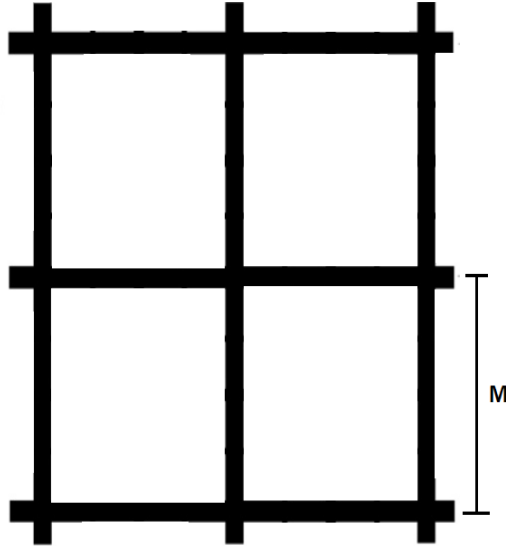
Figure 4.2: Sketch of a section of the grid.

4.2 The model wind turbine

A model wind turbine was placed 3,75 meters downwind on the test section of the wind tunnel. The wind turbine had a diameter of 0,894 meter, and the center of the rotor was located 0,817 meters above the floor level. It has three blades which are connected to a rotating nacelle. The blades can be pitched about the blade quarter chord, but the pitch angle was set to zero in this experiment since this is what the blades are designed for. The nacelle and the blades are connected to a cylindrical hub with a diameter of 0,09 meters. The model blockage ratio, which is defined as the rotor swept area of the turbine divided by the wind tunnel cross-sectional area, was 13 %. This is a little higher than the recommended maximum of 10 %, to avoid tunnel wall interference on the wake expansion [22]. The distance between the tip of the rotor blade and the nearest wall is about 0,6 D, which probably will affect the wake as it develops downstream, but this effect is expected to be small. The tower height to rotor diameter is about the same as a full scale wind turbine, and therefore are interference effects with the ground expected to be about the same. The yaw angle, which is the rotation about the vertical axis of the wind turbine, was set to zero in all the experiments. A picture of the wind turbine is shown in figure 4.3.

The wing profile NREL s826 has been used for the wind turbine blades, designed by National Renewable Energy Laboratory (NREL) in USA for variable speed, pitch–controlled HAWTs. The geometry of the wing profile and the lift and drag coefficients are shown in appendix C, where the chord length and twist angles are also plotted. The design condition for this wing profile is a tip speed ratio of TSR=5 and an angle of attack of $\alpha = 7$.

The nacelle was connected to a transmission belt at the rear of the hub, which transfers moment to a generator located beneath the wind tunnel floor. This generator makes it

Figure 4.3: The wind turbine in the wind tunnel. [21]

possible to control the rotational speed of the turbine through a full-frequency converter. A torque gauge was mounted in the hub to measure the moment about the transmission axis. The torque and rotational speed were used to calculate the power the wind turbine produced, and was then used to find the C_P curve. The sensitivity of the torque transducer was calibrated prior to the test by using calibrated weights applied to the tip of one of the blades when this was locked in a horizontal position. The calibration curve is found in appendix A.1. All the data was logged in the program LabView.

The turbine was also mounted on a force plate such that the thrust force on the turbine could be logged. This was used to find the C_T curve for the wind turbine. The thrust transducer was also calibrated prior to the tests with weight elements of known masses. The calibration curve is found in appendix A.2. The atmospheric pressure was found using a precision mercury manometer and the temperature was logged in LabView from a wall mounted thermometer. The density could then be calculated using the ideal gas law. A sketch of the set up of the different equipment in the wind tunnel is shown in figure 4.4.

The measurements from the pressure transducers, the thrust gauge and the torque gauge were sampled at a frequency of 1000 Hz in 60 seconds, giving a total of 6000 samples for each measurement point. Both mean values and standard deviation values were collected.
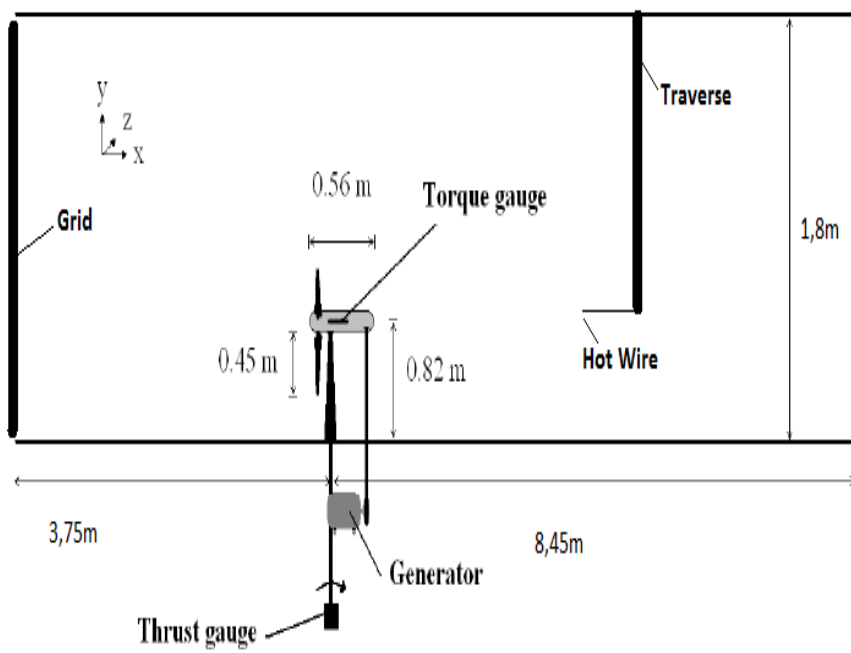
Figure 4.4: The setup of the equipment in the wind tunnel.

4.3 Hot wire probe and anemometer

4.3.1 General hot wire theory

The hot wire anemometer is an instrument which measures fluid velocities up to high frequency fluctuations. It is a common instrument to measure the instantaneous velocity of the flow, and is therefore used to measure fluctuating and turbulent flow. The hot wire anemometer consists of a sensor, a small electrically heated wire exposed to the fluid flow and electrical equipment which transfers the output of the sensor into a useful electrical signal. Typical dimensions of the heated wire are 5 μm in diameter and 1 to 3 mm in length, hence very small and very fragile. The small size of the hot wire disturbs the flow to a minimum. A picture and an illustration of the function of a hot wire probe are shown in figure 4.5 and 4.5.
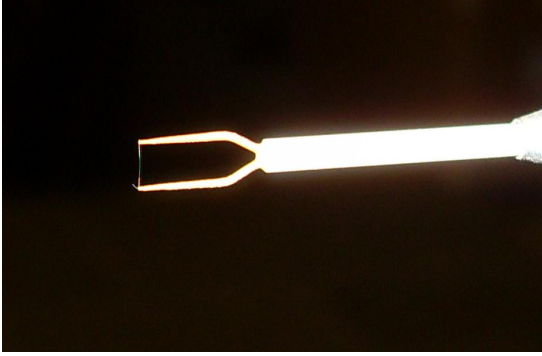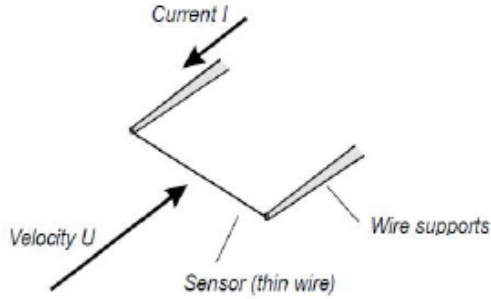

Figure 4.5: Picture of hot wire probe.   Figure 4.6: Function of hot wire.

The heat transfer from the heated wire is a function of the velocity of the fluid flow. The hot wire is most sensitive to wind speeds perpendicular to the wire. The heat transfer from the hot wire can be expressed in terms of an energy balance [25]:

$$q = I^2 R_w = \pi D l h (T_w - T_a) \tag{4.1}$$

where I is the current in the wire, R_w is the hot wire resistance at the operating temperature T_w, T_a is the ambient temperature, D and l the wire diameter and length, respectively, and h is the heat transfer coefficient. The heat transfer coefficient is dependent on properties of the fluid flow, and equation 4.1 can often be expressed as:

$$I^2 R_w = |A + BU^n|(T_w - T_a) = H(U)(T_w - T_a) \tag{4.2}$$

where A represents natural convection and BU^n forced convection. This equation relates the velocity of the fluid to the convective heat transfer of the hot wire. The frequency response from the hot wire anemometer depends on H(U), and it is therefore important to optimize the anemometer response for the mean fluid velocity at which the probe is likely to operate. If the frequency response is flat over a region that covers all the spectrum of frequencies of interest, the instantaneous velocity of the flow can be found. The hot wire is also sensitive to noise, both white noise and noise from other electrical instruments.

This is important to investigate prior to the measurements, and a low-pass filter is often used to filtrate frequencies above the region of interest.

The control circuit in the hot wire anemometer can be either a constant-current circuit or a constant-temperature circuit. A constant temperature circuit has been used in these experiments, because it has a linear response up to much higher frequencies than the constant-current circuit, which is essential to pick up the frequencies in turbulent flow. The temperature of the hot wire is determined by setting the overheat ratio K:

$$K = \frac{R_{w,h}}{R_{w,c}} = 1 + \alpha(T_w - T_a) \tag{4.3}$$

where $R_{w,h}$ is the resistance of the hot wire when it is heated to the temperature T_w, and $R_{w,c}$ the resistance at the ambient temperature T_a. α is an overheating factor which depends on the material of the wire.

4.3.2 Calibration of the hot wire

The calibration curve of a hot wire is non-linear, and has approximately the shape of a 4th-order polynomial with maximum sensitivity at low velocities. The hot wire is calibrated by the use of a pitot tube in a range of different wind speeds. Then a polynomial linearizer is used to find the relation between the output and the wind speed. A fourth order polynomial has been used, and the constants are found by best fit calculations:

$$U = f(E) = k_1 + k_2 E + k_3 E^2 + k_4 E^3 + k_5 E^4 \tag{4.4}$$

where U is the wind speed, E is the voltage output of the hot wire anemometer and k_i are the polynomial constants. The pitot tube is used to find the mean wind speed of the flow, and is first calibrated with a manometer. One of the hot wire calibration curves are found in appendix A.4.

The calibration of the hot wire only lasts for about an hour, and therefore a new calibration had to be done approximately every hour during the measurements. The reason for this is that the hot wires tend to attract dust, and that the high temperature slowly leads to a change of the crystal structure, which affects the resistance of the wire. It is also a good idea to re-calibrate if the temperature changes much in the wind tunnel. The closer the calibration temperature is to the temperature during the measurements, the less temperature correction there is, which also leads to smaller errors.

4.3.3 Experimental setup of the hot wire

The hot wire probe was mounted on a traversing system located behind the model wind turbine. The traverse could be moved in the streamwise (x), vertical (y) and spanwise(z) direction. The probe was pointed perpendicular to the mean flow to measure properties in the streamwise direction, and the wire was horizontal. A pitot static-probe was placed parallel to the hot wire, and was connected to a pressure transducer and then an amplifier

outside of the wind tunnel. The hot wire was connected to an anemometer, which has built-in amplifiers and filters. Both the pitot static-probe and the hot wire anemometer was then connected to a DAQ-board, and the signals were logged in LabView. High frequency noise was filtered out with a low-pass filter, where the filter cut-out frequency was set to 6,5 kHz. Following the sampling rate theorem or Nyquist criteria [7], the sampling rate for the hot wire was set to 13 kHz in this experiment, which is twice the filter cut-out frequency. The sampling time was set to 60 seconds, and both mean values and time series were logged for the hot wire signals.

The hot wire in this experiment had a resistance of $R_{w,c} = 5, 7\,\Omega$ at ambient temperature, and the overheating factor was $\alpha = 1, 69 \cdot 10^{-3}$ 1/°C. An operational temperature of 300 °C was chosen, which gives a theoretical operational resistance of $R_{w,h} = 8, 4\,\Omega$ and an overheat factor of K=1,47 if the ambient temperature is 20 °C.

In this experiment the hot wire was first used to find the turbulence intensity and turbulence length scales generated from the grid in an empty tunnel, and then it was used to find the wake profiles in the wake downstream of the wind turbine. The traverse, which was controlled by a computer, was used to move the hot wire through the wake in the spanwise (z) direction. The wake profiles were measured at the distances $\frac{x}{D}$=1, 3 and 5 downstream of the wind turbine.

The sampled signals from the hot wire and pitot static-probe were stored in text files and imported to a data reduction program based on Fortran. The Fortran script corrects the data for temperature change and fits polynomials to the velocity calibration data. Then the mean, maximum and minimum velocities, the turbulence intensities, the normal stresses, the skewness factor and the flatness factor are calculated for each of the hot wire time series.

4.4   Experimental design

4.4.1   Location of the wind turbine

Before the wind turbine performance and wake measurements could start, the location of the wind turbine in the wind tunnel had to be determined. The hot wire was first used to find the turbulence intensities at the centreline along the tunnel test section, from the grid and backwards in the x-direction. The turbulence intensity at the location 3,5 meters behind the grid was 5,83 %, while at 4 meters behind the grid the turbulence intensity was 5,25 %. Referring to figure 3.5, the turbulence intensity at a free stream wind speed of 10 m/s is approximately 5 %. According to Barthelmie et al.(2012) the turbulence intensity offshore at hub-heights above 50 meters is typically less than 6 % in the wind speed range between 8-12 m/s. It was therefore decided that the turbulence intensities between 3,5 and 4 meters behind the grid were corresponding to atmospheric turbulence intensities offshore, and because of practical reasons the wind turbine was placed 3,75 meters behind the grid. The turbulence intensity decayed to 3,36 % at 8 meters behind the grid.

4.4.2 Performance measurements

The experiments for the wind turbine performance characteristics were first performed without the grid in uniform, steady and parallel flow conditions, and then with the turbulence-generating grid mounted at the entrance of the test section, to generate turbulence to the incoming flow field. The results with and without free stream turbulence could then be compared. The rotational speed of the turbine was varied to obtain different tip speed ratios, while the reference wind speed was kept constant. According to the Norwegian Water Resources and Energy Directorate [10], the annual wind speed at 100 meters above sea level in the Norwegian and Northern European sea areas is approximately 10 m/s. Therefore a reference velocity of about 10 m/s has been chosen for the wind tunnel experiments, and this wind speed is also chosen in many earlier experiments. In addition are the power coefficient curves proven to be independent of the reference wind speed above 9 m/s [23].

4.4.3 Wake measurements

As with the performance characteristics, the wake measurements were first done with close to zero turbulence in the incoming flow field, and then with a turbulence intensity of about $5,5\%$ in the incoming flow, such that these results could be compared. The reference wind speed was constant at approximately 10 m/s.

The hot wire measurements were performed parallel to the rotor plane at the distances $\frac{x}{D}$=1, 3 and 5 downstream of the wind turbine, which is normal practice to see how the wake develops downstream. Horizontal measurements were performed across the wake in the spanwise direction at these three distanced downstream, first without the grid and then with the grid. The traversing system was controlled by a computer, which was used to move the hot wire through the wake. The origin of the coordinate system was set at the centre of the rotor. The measurements were taken at hub-height, and covered an area of 2,4 diameters in the z-direction, hence 1,2 diameters to each side of the centreline. The outer point was then approximately 25 cm from the sidewall, such that the free stream outside the wake was reached, but before the boundary layer from the sidewall was affecting the flow. Prior to the wake measurements, some test measurements were performed in the wake to locate the tip vortices and to figure out the distance between the measurement points. At x=1D the measurement points were taken with 0,5-1 cm intervals in the tip vortices, and 2-3 cm intervals in the middle section. These intervals could be slightly increased further downstream, especially with free stream turbulence. After all the measurements were finished, a computer programme processed the data into values that could be analysed and plotted. The mean velocity profile, the turbulent kinetic energy, the skewness factor and the flatness factor have been plotted and analysed, which will be presented in section 5.3.

Chapter 5

Results and discussion

5.1 Turbulent length scales

After the location of the wind turbine was chosen, the streamwise length scale of the turbulence generated from the grid had to be determined. Hot wire measurements were done at hub hight along the rotor plane, and the frequency spectrum was analysed to find the length scale. The normalized power spectrum (see section 3.2.3) from the hot wire measurements were compared to von Karmans model from equation 3.22, and the approximate length scale was found by adjusting the length scale $^{x}L_u$ until the two curves had the best fit. Figure 5.1 shows the power spectrum compared to von Karman's model with a length scale of $^{x}L_u = 0,12$, but this value is only approximate. Auto-correlation calculations resulted in a length scale closer to $^{x}L_u = 0,2$ meters.
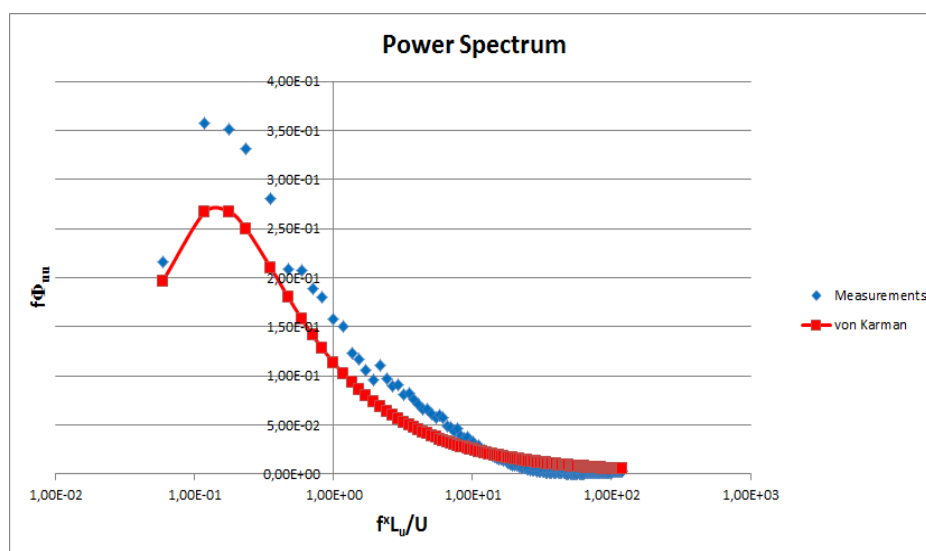

Figure 5.1: Power spectrum for the experimental data compared to von Karman's model.

Many full scale wind turbines have a hub height of about 80 meters. According to equation 3.19 the length scale at this height, with a surface roughness for open sea of $z_0 = 0,001$

meters [17], is $^{x}L_u = 179$ meters. The model wind turbine in the wind tunnel has a hub hight which is approximately $\frac{1}{100}$ of a full-scale wind turbine, which gives a scaled length scale of $^{x}L_u = 1,79$ meters. This calculated length scale is only an estimate and depends on the surface roughness, and from experience a length scale of 179 meters at an elevation of 80 meters seems like an over-prediction. A length scale closer to 100 meters would probably be more reasonable [18]. However, the length scale of $^{x}L_u = 0,02$ meters produced from the grid in the wind tunnel is much smaller, about 5-6 times, than what is expected relatively to a full-scale wind turbine. This means that the relative sizes of the vortices in the wind tunnel are smaller than what a full-scale wind turbine experiences offshore. The effect of this is that a smaller part of the model wind turbine will be affected by the vortices, compared to a full-scale turbine. Hence, the turbulence produced by the grid in the wind tunnel will probably have a weaker effect on the model wind turbine's performance characteristics and wake development compared to a full-scale turbine in the atmospheric boundary layer. However, the grid turbulence in the wind tunnel clearly has an effect on the results, as will be presented in section 5.2 and 5.3.

5.2 Performance characteristics

5.2.1 Power coefficient curves

The power coefficient curves from the lab experiment have been calculated as in equation 2.15, where the power P is the product of the torque Q and the rotational speed Ω: $P_{extracted} = Q \cdot \Omega$. The tip Reynolds number $Re = \frac{\omega R c}{\nu}$ changed from about $Re = 3,5 * 10^4$ for $\lambda \approx 2$ to $Re = 2,0 * 10^5$ for $\lambda \approx 11$. The C_P curves with and without grid turbulence are shown in figure 5.2. The low values of the power coefficient at low tip speed ratios are due to effects of stall, which results in a loss of lift and increase of drag. At high tip speed ratios there is a development of negative angles of attack on the inner section of the blade. This causes power to be transmitted to the flow rather than being extracted from it, which leads to low power coefficient values. The runaway point, where the turbine no longer extracts energy from the flow, occurs at a tip speed ratio of about $\lambda \approx 11,1$ without grid turbulence and $\lambda = 10,9$ with grid turbulence.

The peak power coefficient is $C_P = 0,461$ at $\lambda = 5,44$ without the grid and $C_P = 0,45$ at $\lambda = 5,74$ with the grid. This peak value is therefore 2,4 % lower when free stream turbulence is present, and the effect of turbulence is strongest when the turbine is operating in optimal conditions. For low tip speed ratios the two curves in figure 5.2 are mostly overlapping, which means that the effect of stall is dominant in this region. In this deep stall region, at high angles of attack, the lift coefficient is approximately constant and the free stream turbulence does not affect the power extraction of the turbine. For high tip speed ratios the two C_P curves are almost overlapping, but the power coefficient with grid turbulence tends to be a little lower than without the grid. The conclusion is therefore that free stream turbulence has a negative effect on the power coefficient when the blades are not stalled, and this effect is largest when the wind turbine is operating in optimal conditions. However, the effect of free stream turbulence on the power coefficient is relatively small, with a maximum deviation of 2,4 %.
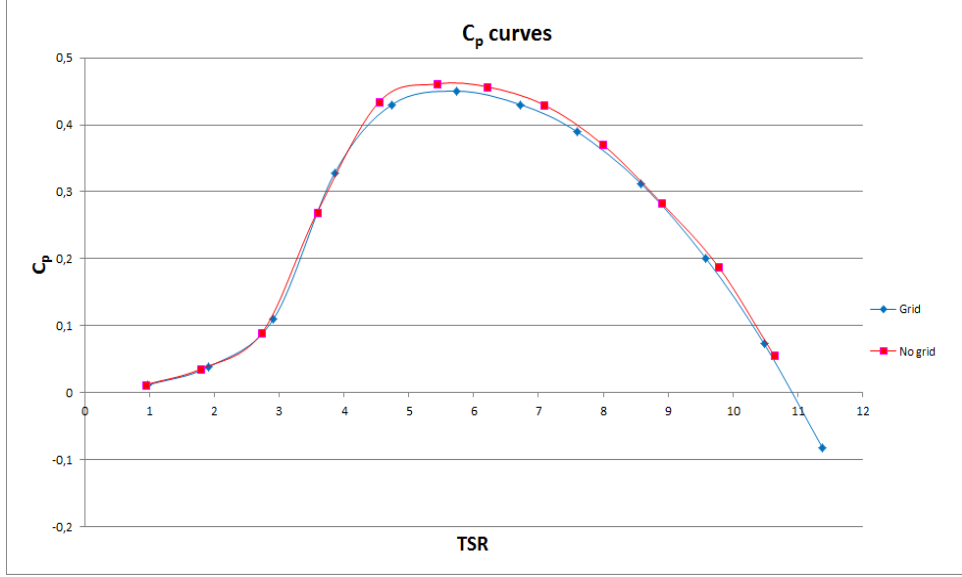
Figure 5.2: C_P curves with and without grid turbulence.

There are two effects of the free stream turbulence which can have an effect on the power coefficient when the blades are not stalled. First, the incoming turbulent flow makes the flow in the boundary layer surrounding the blades transform to a turbulent boundary layer faster. This increases the boundary layer thickness and hence also the drag. Second, when the incoming flow field is turbulent, the relative velocity at the blades changes and the angles of attack on the turbine blades are changed frequently. The incoming turbulent flow field is three dimensional, and there are fluctuating components in all three dimensions, as described in equation 3.3, 3.4 and 3.5. The power extracted from the wind turbine is a function of the lift coefficient, the drag coefficient, the rotational speed, the angle of relative wind and the relative velocity that the blades see:

$$P \propto (C_l \sin \phi - C_d \cos\phi) \, U_{rel}^2 \, \Omega \tag{5.1}$$

Increased drag will therefore reduce the power. For a uniform, non-turbulent flow field, the relative velocity can be expressed as $U_{rel}^2 = U_{ref}^2 + (\Omega r)^2 = U_{ref}^2(1+\lambda^2)$ if the induction factors are neglected, see illustration in figure 2.4. If the incoming flow field is turbulent, the fluctuating part of the velocity also has to be included:

$$U_{rel}^2 = (U_{ref} + u')^2 + (\Omega r + v')^2 \simeq U_{ref}^2 + u'^2 + (\Omega r)^2 + v'^2 \tag{5.2}$$

As can be seen from equation 5.2, turbulence is increasing the relative velocity, which again is increasing the power extraction. Hence, there are two opposite effects of turbulence on the power coefficient, the increased drag is reducing the power while the increased relative velocity squared is increasing the power extraction. This may be the reason why the difference between the two C_P curves in figure 5.2 is so small, even though the difference in the turbulence intensity of the incoming flow is about 5,5 %. However, since the C_P curve with free stream turbulence is a little lower, it seems like the effect of drag is slightly higher than the effect of increased relative velocity. The dynamic effects of the turbulent incoming flow hence decrease the power extraction of the turbine, and the effect of this is strongest around the peak of the C_P curve.

However, the differences in the two curves in figure 5.2 were smaller than expected, and the reason for this may be the boundary layer developed from the grid laying on the floor in the measurements without free stream turbulence. This boundary layer may have disturbed the flow at the tip of the blade closest to the ground, and it may also have affected the correlation factor between the velocity from the contraction and the reference velocity. An improvement of the experiment would therefore be to completely remove the grid from the tunnel when the measurements without grid turbulent are to be conducted. Another reason may be that the length scale of the turbulence generated from the grid is much smaller than what would have been expected on a wind turbine in the free atmosphere. This might be reducing the effect of the free stream turbulence acting on the wind turbine and on the wake downstream.

According to the error analysis performed as in appendix D, the uncertainty in the peak C_P value with and without grid are $\pm 0,9\%$ and $\pm 1,0\%$, respectively, with a confidence interval of 95 %. The uncertainty in the reference wind speed was estimated to $\pm 0,6\%$. These calculated uncertainties are probably slightly underestimated, since the values of some of the possible errors were unknown and neglected. Anyway, the uncertainty seem to be lower than the difference between the two peak C_P values in figure 5.2.

5.2.2 Thrust coefficient curves

The thrust coefficients are calculated as in equation 2.17. The drag force acting on the tower and nacelle system without the blades has previously been measured to a drag coefficient of $C_D = 0,137$ [23]. The effective thrust force was therefore calculated by subtracting the tower and nacelle system drag from the thrust on the whole system. The results for the thrust coefficients with and without grid turbulence are shown in figure 5.3. The curves are very similar both with and without grid, but the thrust coefficient with grid turbulence tends to be marginally higher, especially at high tip speed ratios. At $TSR = 6$, where the power coefficients are peaked, the thrust coefficient without grid turbulence is $C_T \approx 0,89$, which is 2,1 % lower than with grid turbulence at $C_T \approx 0,91$. The velocity deficit just behind the rotor should therefore be very similar both with and without free stream turbulence. The conclusion is therefore that free stream turbulence has a relatively small effect on the performance characteristics of the model wind turbine. The effect of free stream turbulence on the wake development downstream will be considered in section 5.3.
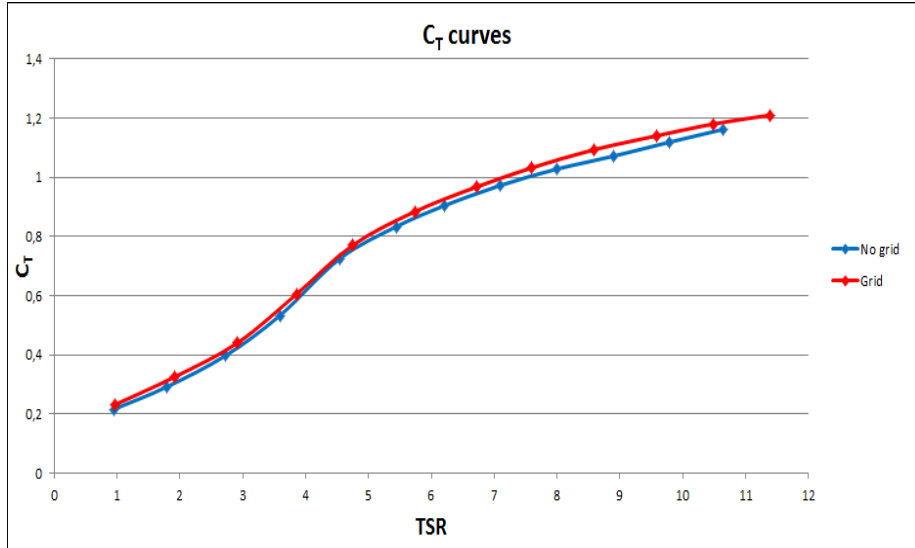
Figure 5.3: C_T curves with and without grid turbulence.

5.3 Wake profiles

The wake development behind wind turbines gives information both on power losses in turbine parks, as well as on increased turbulence levels which may be affecting flow-induced rotor loads. The main characteristics of the wake are the mean velocity deficit and the tip vortices shed by the blades forming three spiral vortices downstream of the turbine. During all the wake measurements the wind turbine operated at the optimal tip speed ratio $\lambda \approx 6$, since this region, according to the C_P curves in figure 5.2, was seen to be most sensitive to changes in the free stream turbulence level. When the turbine is operating at it's design condition, the pressure drop across the rotor is almost uniform [21]. Hence, one might expect the initial wake profile to be top hat shaped and the turbulent stresses to be small except for near the tip and the root.

5.3.1 Mean velocity deficit profiles

The mean velocity profiles are plotted as the deviation from the free stream velocity: $1 - \frac{U_{mean}}{U_{ref}}$. These profiles are shown in figure 5.4, 5.5 and 5.6 for x=1D, x=3D and x=5D downstream of the turbine, respectively. The length scale on the horizontal axis of the plots is the z-position normalized with the turbine blade's radius R. The velocity deficit is largest just behind the rotor and decreases further downstream due to the entrainment of air from outside the wake through turbulent diffusion.

The velocity profiles at x=1D are approximately top-hat shaped as expected, due to the uniform pressure drop across the rotor at TSR=6. The asymmetry of the wake profiles in figure 5.4 is due to disturbances in the flow from the tower and nacelle. The dip close to the centreline is partly due to flow acceleration caused by displacement effects from the nacelle, and partly because the blades do not extend all the way into the nacelle,

41

such that there is no energy extraction here. The velocity deficit just behind the rotor is directly connected to the thrust coefficient of the turbine, since this determines the momentum extracted from the flow. The thrust coefficient with free stream turbulence is only marginally higher than without free stream turbulence, and it was therefore expected that the mean velocity profiles at x=1D should be very similar. From figure 5.4 it is seen that the mean velocity profiles are almost identical, the velocity deficit with free stream turbulence is just slightly higher than the other. This is as expected and the same result was found in a study by Medici & Alfredsson (2006) [30].

Further downstream, at x=3D and x=5D, the velocity deficit is decreasing and the velocity profiles become more curve shaped. The mean velocity profiles with free stream turbulence are broader and more smeared out than without free stream turbulence, as expected. The asymmetry seen as the small peak on the right hand side of the profiles in 5.5 and 5.6 is probably due to footprints from the tower wake. At x=5D the disturbance in the flow because of the tower is still seen at the profile without the grid, but this is smeared out with the grid. It is therefore seen that the velocity profiles become flatter and more homogeneous with higher levels of turbulence.

The turbulent flow's ability to smear out velocity gradients and inhomogeneities can be explained from the equation for the evolution of turbulent kinetic energy in section 3.2.4. The turbulent diffusion term in equation 3.24 is dependent on the velocity gradients in the wake, and the velocity gradients are strongest in the radial direction. This means that the transfer of momentum also is strongest in the radial direction, and this radial diffusion increases with the level of turbulence in the free stream. Figure 5.5 and 5.6 clearly show that the free stream turbulence is smearing out inhomogeneities in the flow faster, and the velocity profile also becomes flatter and broader faster when free stream turbulence is present.

However, the two profiles in figure 5.5 and 5.6 were expected to differ even more. The reason for this might be the boundary layer created from the grid laying on the floor in the measurements without free stream turbulence. This boundary layer has most likely grown into the wake downstream in the wind tunnel, and may have disturbed the flow here. Another reason may be that the length scale of turbulence generated from the grid is much smaller than what would have been expected on a wind turbine in the free atmosphere. This might be reducing the effect of the free stream turbulence acting on the wind turbine and on the wake downstream.
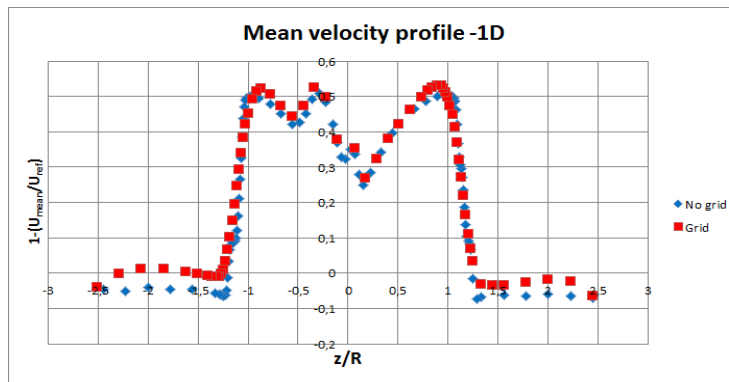
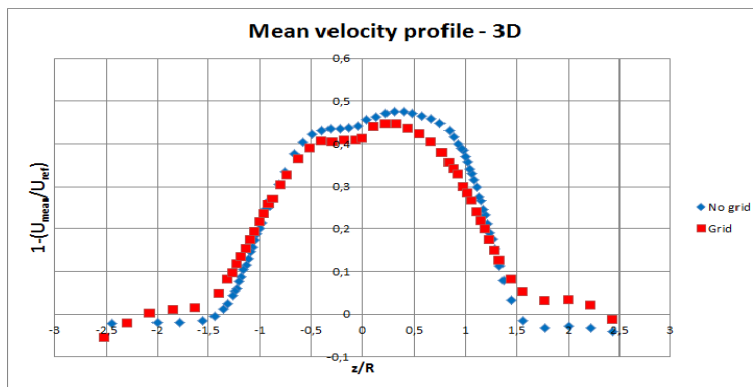Figure 5.4: Velocity profile of the wake x/D=1 downstream. $U_{ref} = 10,2 - 10,3$ m/s.

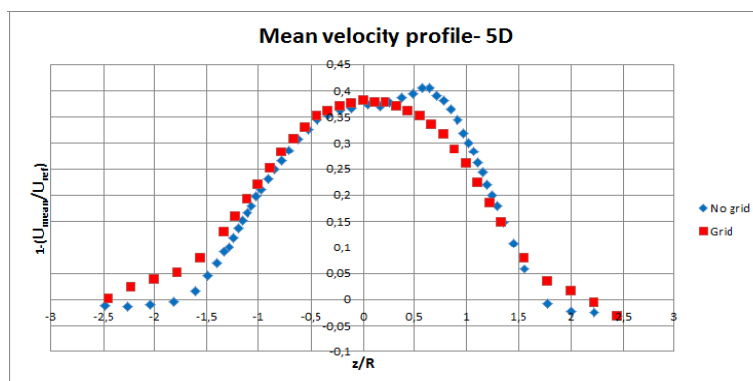Figure 5.5: Velocity profile of the wake x/D=3 downstream. $U_{ref} = 10,2 - 10,3$ m/s.

Figure 5.6: Velocity profile of the wake x/D=5 downstream. $U_{ref} = 10,2 - 10,3$ m/s.

5.3.2 Turbulent kinetic energy profiles

The turbulent kinetic energy is defined in equation 3.23, but only the normal stresses in the streamwise direction, $\overline{u'u'}$, were measured in this experiment. The normal stresses in all three dimensions have been measured in an earlier experiment for the same model wind turbine at x=1D downstream of the turbine with a tip speed ratio of 6 and with low turbulent, uniform incoming flow [24]. These normal stresses and the turbulent kinetic energy are shown in figure 5.7, and it is clear that the flow is anisotropic. It is seen that all of the three normal stresses are within the same order of magnitude, but it is smallest in the rotational direction and highest in the radial direction. The normal stress in the streamwise direction is approximately in between, and the turbulent kinetic energy is therefore approximately $k \simeq \frac{3}{2}\overline{u'u'}$. This approximation has been used to calculate the kinetic energy from the streamwise normal stresses.
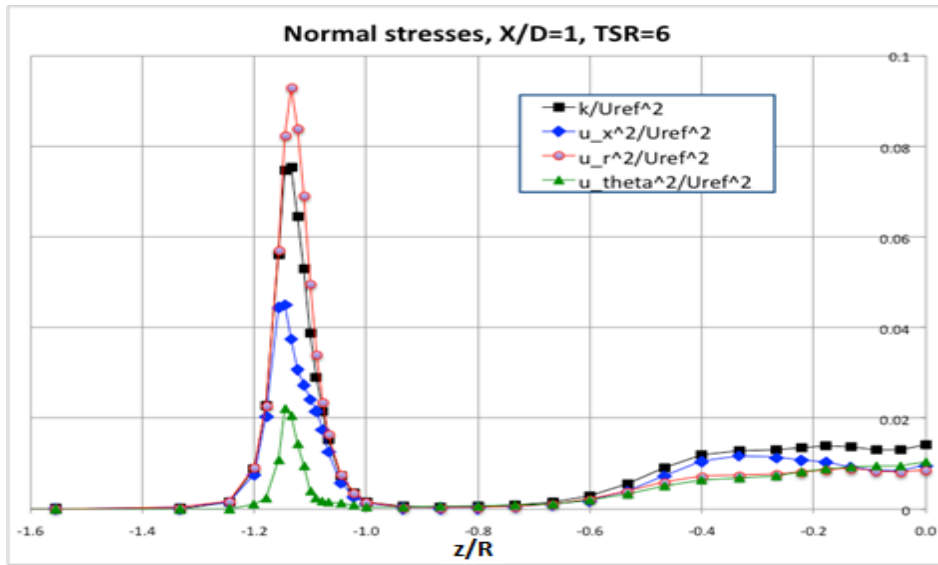

Figure 5.7: Normal stresses in the wake at TSR=6 and x=1D.

The turbulent kinetic energy in the wakes are normalized by the reference velocity squared: $\frac{k}{U_{ref}^2}$. The plots for the three different downstream distances are shown in figure 5.8, 5.9 and 5.10. The peaks on each side indicate the tip vortices from the tip of the blades. The peak to the right is slightly higher than the peak to the left, and this is probably because there is a banner on the left sidewalls, which gives a different surface roughness than the right sidewall. There are also high turbulence levels behind the hub, and the asymmetry here is due to disturbances from the tower and nacelle.

The peak kinetic energy is highest at $\frac{x}{D}$=1, and decreases downstream due to dissipation and diffusion of turbulent energy. As described from the energy cascade in section 3.2.4, the eddies that are formed break up and transfer energy into smaller and smaller eddies until the energy is dissipated by viscous action at the Kolmogorov scale. This leads to a decay of the kinetic energy downstream. At x=3D and x=5D the turbulent energy distribution across the wake has been smoothed by spanwise turbulent diffusion and the peaks generated from the tip vortices are less distinct than at x=1D. In section 5.3.1 it

was explained that increased levels of turbulence increases the radial transport of energy in the wakes. In figure 5.8, 5.9 and 5.10 the peak kinetic energy is lower with free stream turbulence, and the increased turbulence diffusion has also smeared out the peaks.

However, at x=1D the peaks in the kinetic energy from the tip vortices are lower with free stream turbulence, but the rest of the profile in figure 5.8 is not that smeared out and almost identical to the profile without free stream turbulence. This was unexpected, because the total amount of energy across the tunnel cross-section should be the approximately constant, since the power and thrust coefficients with and without free stream turbulence are almost the same. The profile with grid turbulence was expected to be more smeared out than what is seen in figure 5.8, and the reason for this lack in the spread of energy is unknown. The kinetic energy with free stream turbulence tends to be a little higher than without free stream turbulence close the walls and in the middle section, but it does not seem to add up for the difference in energy in the tip vortices. Since there are no clear reasons for this, it should be investigated further, and the experiment at x=1D should be repeated to assess whether the profiles in figure 5.8 are correct or not.
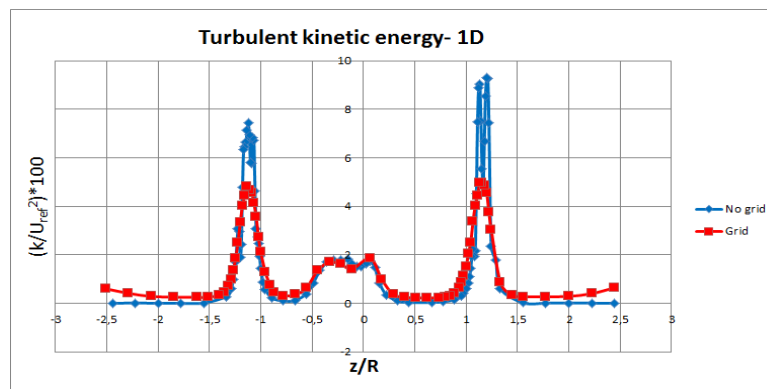

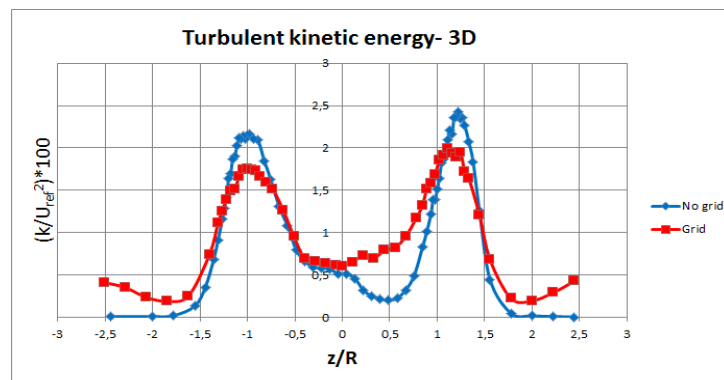Figure 5.8: Turbulent kinetic energy in the wake x/D=1 downstream.

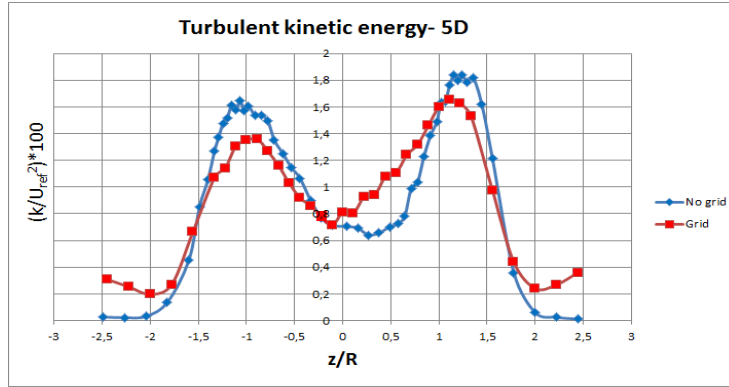Figure 5.9: Turbulent kinetic energy in the wake x/D=3 downstream.

Figure 5.10: Turbulent kinetic energy in the wake x/D=5 downstream.

5.3.3 Skewness factor

Figure 5.11, 5.12 and 5.13 show the skewness factors for the velocity distribution in the streamwise direction at x=1D, 3D and 5D downstream of the wind turbine, respectively. An explanation of the skewness factor can be found in section 3.2. At x=1D the skewness factor is relatively close to zero just behind the rotor, and this is probably because the vortices shed from upper and lower surfaces at the blades have approximately equal strength, but opposite directions at TSR=6. It seems like these two vortices have almost cancelled each other out already at x=1D. This means that the velocity distribution is relatively symmetric in this region, both with and without free stream turbulence.

Not surprisingly are the tip vortices resulting in the largest changes of the skewness factors across the wake. In the tip vortices at x=1D the skewness factor is varying between negative and positive values, due to negative and positive contributions from the vortices. At x=3D and x=5D it is clearly seen that the tip vortices are stretched out and wider than at x=1D. This is seen as the skewness factor becomes more spread out, and the positive contribution moves towards the centre of the rotor, while the negative contribution moves towards the walls. The skewness factor profiles are relatively symmetric, but there are some small asymmetries in the midsection due to the tower wake, root vortices and disturbances from the nacelle. The asymmetries are less present with free stream turbulence, which also shows that increased levels of turbulence are smearing out velocity gradients and inhomogeneities faster.

The stretching of the tip vortices hence leads to a more or less positive skewness factor in the mid-section of the wake at x=3D and x=5D, while it drops to negative skewness factors further out in the radial direction. A positive skew is, as explained in section 3.2, leaned to the left of the mean value, with longer and thicker tails to the right. This is proven to be correct as a simplified probability density function has been made for one of the measurement points with a positive skewness factor of $S_u = 0,698$, which is shown in figure 5.15. The horizontal axis is the mean velocity U_{mean} subtracted from the instantaneous velocity u, hence the fluctuation u', and it is ordered in bins. Comparing figure 5.15 to the simplified probability density function in figure 5.14, with a negative skewness factor of $S_u = -1,329$, it is clear that the positively skewed distribution is leaned to the left while the negatively skewed distribution is leaned to the right. A

positive skew hence means that a large portion of the fluctuations are negative and lower than the mean wind speed at this point, but the most extreme fluctuations are positive, hence the longer and fatter tail to the right. The opposite applies to a negative skew. The peakedness of the curves increases with the flatness factor, as will be more discussed in the next section. However, it is seen that with free stream turbulence the transfer from positive to negative skewness factors across the wake are more smoothed as expected.

The conclusion is therefore that the velocity distribution in the wake of a wind turbine is mostly skewed and not symmetric. Hence, the velocity distribution in the wake is non-Gaussian due to the tip vortices and the disturbances from the tower, nacelle and root vortices. However, the skewness factor is approaching zero as the wake develops downstream, and the wake will eventually become approximately isotropic and Gaussian further downstream. This applies both to the measurements with and without free stream turbulence, but the free stream turbulence is smearing out the variations and the inhomogeneities in the skewness factor across the wake faster. In addition are the most extreme values of the skewness factor lower with free stream turbulence, which means that the velocity distribution is less asymmetric at these points. This is due to the more efficient mixing and faster recovery with increased levels of turbulence.
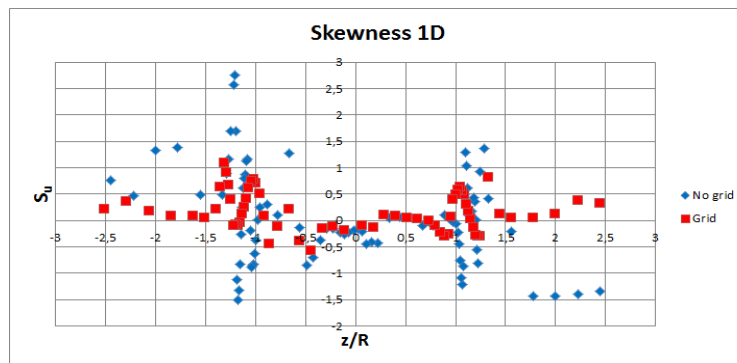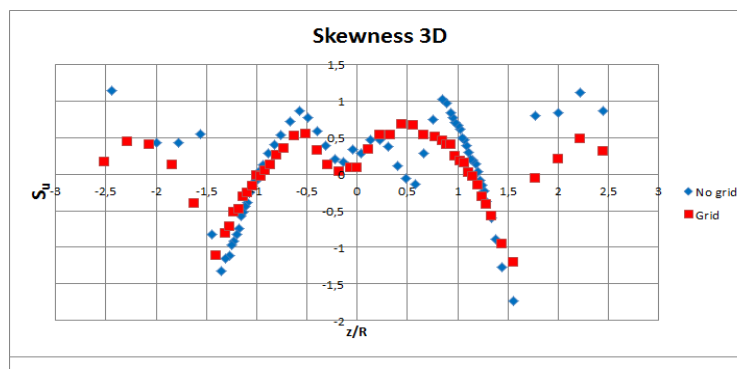

Figure 5.11: Skewness of the wake x/D=1 downstream.
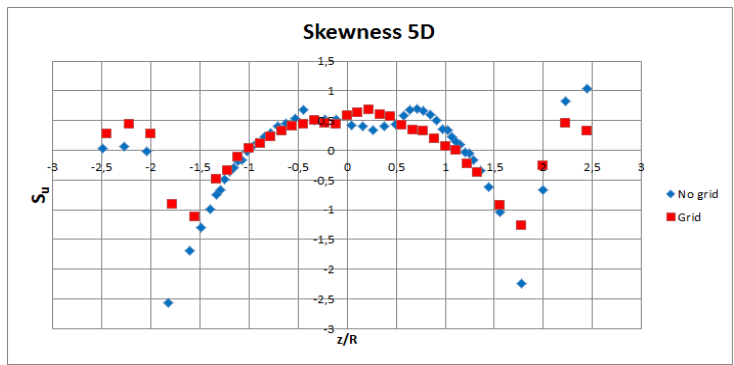

Figure 5.12: Skewness of the wake x/D=3 downstream.
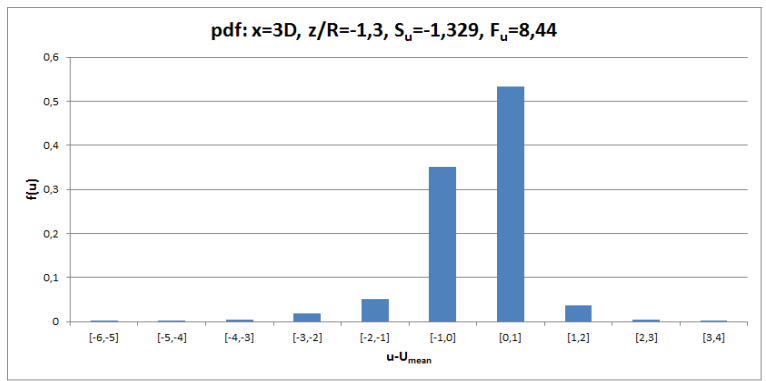
Figure 5.13: Skewness of the wake x/D=5 downstream.

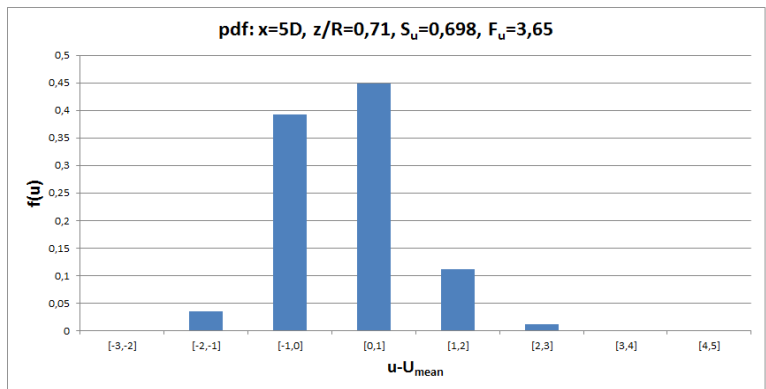Figure 5.14: Simplified pdf of velocity distribution at x=3D without grid at z/R=-1,3. S_u=-1,329, F_u=8,44.

Figure 5.15: Simplified pdf of velocity distribution at x=5D without grid at z/R=0,71. S_u=0,698, F_u=3,65.

5.3.4 Flatness factor

Figure 5.16, 5.17 and 5.18 show the flatness factors for the velocity distribution in the streamwise direction at x=1D, 3D and 5D downstream of the wind turbine, respectively. An explanation of the flatness factor can be found in section 3.2. As with the skewness factor, the variation of the flatness factor is largest without free stream turbulence, and the variation decreases further downstream behind the wind turbine. The flatness factor is close to 3 in a large part of the measurements, except in the tip vortices. The Gaussian distribution has a flatness factor of F=3, which means that the peak of the velocity distribution in a large part of the wake has the same flatness as the Gaussian distribution. A velocity distribution with a flatness factor of $F_u = 3,65$ is shown in figure 5.15, while a velocity distribution with a flatness factor of $F_u = 8,44$ is shown in figure 5.14. It is seen that the distribution with the highest flatness factor has a higher and more distinct peak.

The tip vortices have a high positive flatness factor, which means a more distinct peak in this area than in the rest of the wake. The peak flatness factor in the tip vortices decreases downstream due to vortex stretching and mixing with the surrounding flow. At x=1D the flatness factor is varying the most, while an increased portion of the measurements approaches a flatness factor of 3 further downstream. This development is faster with free stream turbulence, as expected, and the free stream turbulence is again seen to smear out the inhomogeneities across the wake faster as it develops downstream. Hence, the increased radial transport due to turbulent diffusion makes the wake recover faster, which probably will increase the power extraction and reduce the fatigue loads for a possible downwind wind turbine.
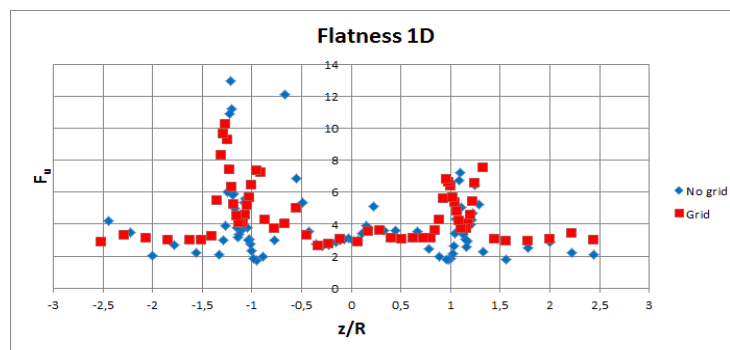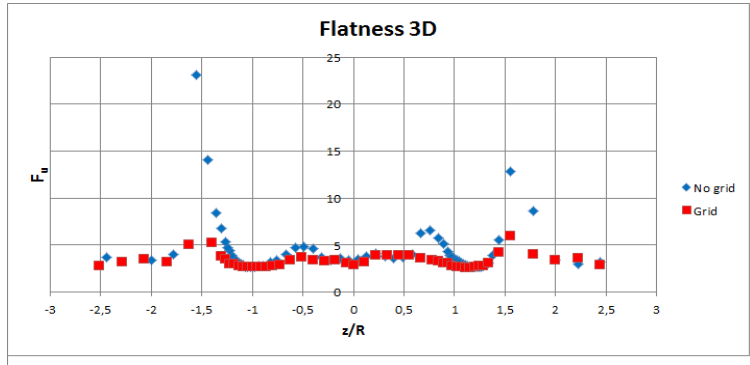

Figure 5.16: Flatness of the wake x/D=1 downstream.
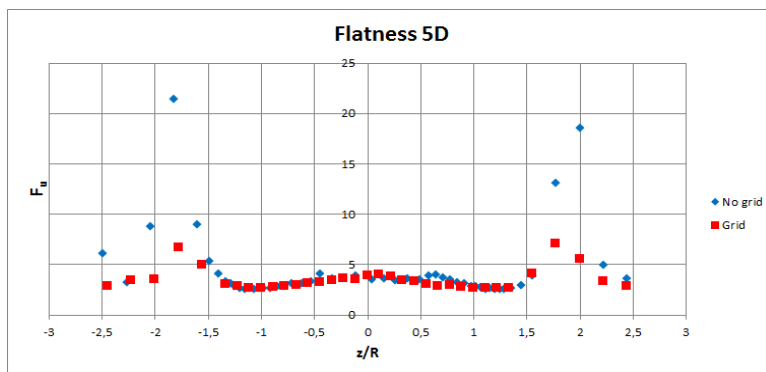
Figure 5.17: Flatness of the wake x/D=3 downstream.

Figure 5.18: Flatness of the wake x/D=5 downstream.

Chapter 6

Conclusion

The experiments in this Master Thesis show that the power coefficient without free stream turbulence is slightly higher compared to the results with a free stream turbulence intensity of 5,5 %, except at low tip speed ratios where the effect of stall dominates. The largest difference in the power coefficients is found at $TSR \approx 6$, which is where the wind turbine operates most efficiently. The peak power coefficient is 2,4 % lower with free stream turbulence, and the reason why this difference is so small is probably because there are two opposite effects of turbulence. If the turbulence level of the incoming free stream increases, it leads to an increase of the drag at the turbine blades, hence reducing the power extraction at the turbine. However, the power is proportional to the square of the relative velocity, which increases with the level of turbulence. Since it seems like the total effect of free stream turbulence is a small reduction of the C_P values, it is reasonable to conclude that the effect of the increased drag has the largest effect on the power coefficient.

The wake measurements show that the effect of free stream turbulence is largest further downstream in the wake. Just behind the rotor, at x=1D, the mean velocity deficit is almost identical both with and without free stream turbulence. This was expected, because the corresponding thrust coefficients were also almost identical, and the momentum deficit is directly connected to the thrust coefficient. Further downstream, at x=3D and x=5D, it is clearly seen that the velocity deficit and the kinetic energy is more smeared out with free stream turbulence. This is caused by increased turbulent diffusion, where higher levels of turbulence leads to an increased transport of radial momentum. Both velocity gradients and inhomogeneities are smeared out faster, and the wake profiles become broader and flatter.

The velocity distribution in the wake is proved to be skewed and kurtotic, hence non-Gaussian, especially in the tip vortices. However, the skewness factor and flatness factor approaches Gaussian values further downstream, and higher levels of turbulence is speeding up this process. The conclusion is therefore that the wake is substantially changed by the presence of free stream turbulence. The recovery of the velocity defects is faster owing to a higher energy mixing and a shorter persistence of the tip vortices. However, the effect of the free stream turbulence both on the performance characteristics and on the wake profiles were lower than expected. This may be due to disturbances from the

boundary layer from the grid laying on the floor in the measurements without grid turbulence, or because the turbulence length scale generated from the grid was smaller than desired.

The turbulence length scale generated from the grid in the wind tunnel is approximately 0,2 meters, which is approximately 5-6 times lower than what would have been expected in the atmospheric boundary layer. This means that the vortices generated from the grid in the wind tunnel are smaller and will probably affect a smaller part of the wind turbine compared to a full-scale wind turbine in the free atmosphere. This may reduce the effect of free stream turbulence on the performance characteristics and wake development for the model wind turbine in the wind tunnel, compared to a wind turbine in the atmospheric boundary layer.

The main conclusions from this Master Thesis are therefore that free stream turbulence has a relatively small effect on the performance characteristics of a wind turbine, and that higher levels of turbulence leads to faster recovery of the wake downstream of the turbine due to increased mixing. Even though the power extraction is slightly reduced with free stream turbulence, it seems like the effect on the recovery of the wake is larger, which will lead to higher power extraction and lower fatigue loads on a downwind wind turbine. Increased levels of atmospheric turbulence will therefore probably increase the total power output in a wind farm. For offshore wind farms the ambient turbulence is often lower than on shore, leading to more persistent wakes. Hence, the total power losses in a wind farm due to wind turbine wakes may be higher offshore than on shore because of lower levels of turbulence.

6.1 Further work

The length scale of the turbulence generated by the grid is, as explained, smaller than what is expected for a wind turbine in the free atmosphere. It would therefore be interesting to further investigate the effect of this turbulent length scale with sizes more comparable to what a full-scale turbine would experience. This could either be done by increasing the grid mesh size, but the dimensions of the wind tunnel would then be the limiting factor. Another solution would be to test a wind turbine of smaller dimensions with the same grid dimensions as used in this Master Thesis.

Both the experiments on the performance characteristics and the wake measurements performed in this Master Thesis resulted in a smaller difference than expected when comparing the results with and without free stream turbulence. As explained in the report, one of the reasons for this may be the boundary layer developed from the grid laying on the floor, and a suggestion to an improvement of the experiment is therefore to completely remove the grid from the wind tunnel when measurements without free stream turbulence are performed.

In figure 5.8 there seems to be a lack of energy, and also a lack in the spread of energy, in the profile with free stream turbulence, compared to the one without free stream turbulence. The reason for this is not clear to the author of this report, and it may be an

indication that something is wrong with the measurements. It could therefore be a good idea to re-do the wake measurements at x=1D to assess whether the profiles in figure 5.8 are correct or not. Also, in this Master Thesis only the velocities and normal stresses in the streamwise direction in the wake has been measured. A suggestion for further work could therefore be to measure the effects of the free stream turbulence in all three dimensions.

Experiments are typically conducted on model wind turbines in wind tunnels because of the high expenses of performing experiments on full-scale wind turbines. Even though many of the same effects are seen on a model turbine and a full-scale turbine, the results will suffer from scaling-effects, and atmospheric turbulence differs from turbulence generated in a laboratory. In the atmosphere, convective turbulence coexists with mechanical turbulence. The Reynolds number will also typically be higher at the full-scale turbine, which will have an influence on the boundary layer development at the turbine blades. While the incoming flow field is relatively uniform across the rotor of a model wind turbine in a wind tunnel, the diameter of a full-scale wind turbine can be up to more than 100 meters, which gives differences in the vertical wind shear from the lower to the upper tip of the rotor. The shear and turbulence intensity are observed to be higher at the top tip of the turbine. An ideal experiment would therefore be to measure the effect of atmospheric turbulence on a full-scale wind turbine in the free atmosphere. This is not possible for most researchers, but it would be interesting to further investigate if the results from this report are comparable to results from larger wind turbines in an open environment.

Bibliography

[1] J.F. Manwell, J.G. McGowan, A.L. Rogers, *Wind Energy explained*, 2nd edition, Wiley, 2009

[2] F. M. White, *Fluid Mechanics*, 6th edition, McGraw-Hill, 2008

[3] S. B. Pope, *Turbulent flows*, Cambridge University Press, 2000

[4] International Energy Agency, *World Energy Outlook 2012*, November 12th 2012.

[5] Global Wind Energy Counsil, *Offshore Wind*, http://www.gwec.net/global-figures/global-offshore/, May 2013.

[6] M.O.L. Hansen, *Aerodynamics of Wind Turbines*, 2nd edition, Earthscan, 2008

[7] A. J. Wheeler, A. R. Ganji, *Introduction to engineering experimentation*, 3rd edition, Pearson, 2004

[8] E. Simui, R. H. Scanlan, *Wind effects on structures: An introduction to wind engineering*, John Wiley & Sons, 1978

[9] T. Burton, D. Sharpe, N. Jenkins, E. Bossyanyi, *Wind Energy Handbook*, John Wiley & Sons, 2001

[10] Norwegian Water Resources and Energy Directorate, *Offshore wind power in Norway*, 2010

[11] K. S. Hansen, R. J. Barthelmie, L. E. Jensen, A. Sommer, *The impact of turbulence intensity and atmospheric stability on power deficits due to wind turbine wakes at Horns Rev wind farm*, Wind Energy 2012, **15**:183–196

[12] R. J. Barthelmie, K. S. Hansen, S. C. Pryor, *Meteorological Controls on Wind Turbine Wakes*, Proceedings of the Institute Electrical and Electronics Engineers, 2012

[13] R. J. Barthelmie, S.T Frandsen, M.N. Nielsen, S.C. Pryor, P.E. Rethore, H.E. Jørgensen, *Modelling and Measurements of Power Losses and Turbulence Intensity in Wind Turbine Wakes at Middelgrunden Offshore Wind Farm*, Wind Energy 2007, **10**:517-528,

[14] M. Turk, S. Emeis, *The dependence of offshore turbulence intensity on wind speed*, Journal of Wind Engineering and Industrial Aerodynamics, 2010

[15] F. Porté-Agel, Y.-T. Wu, H. Lu, R. J. Conzemius, *Large-eddy simulation of atmospheric boundary layer flow through wind turbines and wind farms*, Journal of Wind Engineering and Industrial Aerodynamics, 2011

[16] Y.-T. Wu, F. Porte-Agel, *Atmospheric Turbulence Effects on Wind-Turbine Wakes: An LES Study*, Energies 2012, **5**:5340-5362;

[17] J. Counihan, *Adiabatic atmospheric boundary layers: A review and analysis of data from the period 1880-1972*, Atmospheric Environment 1975, **9**:871-905.

[18] P.-Å. Krogstad, Supervisor

[19] P.-Å. Krogstad, P.A. Davidson, *Is grid turbulence Saffman turbulence?*, J. Fluid Mech. 2010, **642**:373-394

[20] P.-Å. Krogstad, P.A. Davidson, *Homogeneous turbulence generated by multi-scale grids*, J. Phys 2011, **318**

[21] P.-Å. Krogstad, P. E. Eriksen, *"Blind test" calculations of the performance and wake development for a model wind turbine*, Renewable Energy 2013, **50**:325-333

[22] P.-Å. Krogstad, M. S. Adaramola, *Performance and near wake measurements of a model horizontal axis wind turbine*, Wind Energy 2012, **15**:743-756

[23] P.-Å. Krogstad, J.A. Lund, *An experimental and numerical study of the performance of a model turbine*, Wind Energy 2011

[24] P.-Å. Krogstad, *About the NTNU model turbine data base and the two blind tests*, Internal power point presentation

[25] T. Arts, H. Boerrigter, J.-M. Buclin, M. Carbonaro, G. Degrez, R. Dénos, D. Fletcher, D. Olivari, M.L. Riethmuller, R.A. Van den Braembussche, *Measurement techniques in fluid dynamics, An introduction*, von Karman Institute for Fluid Dynamics, 2004, 2nd revised edition

[26] A.L. Kistler, T. Vrebalovich, *Grid Turbulence at large Reynolds numbers*, J. Fluid Mech. 1966, **26**:37-47

[27] Kjersti Røkenes, *Investigation of terrain effects with respect to wind farm siting*, Doctoral thesis at NTNU, 2009

[28] Warren M. Hagist, Leif N. Persen, *Turbulence-An introductory course*, NTNU, 1975

[29] L.J. Vermeer, J.N. Sørensen, A. Crespo, *Wind turbine wake aerodynamics*, Aerospace Sciences 2003, **39**:467–510

[30] D. Medici, P.H. Alfredsson, *Measurements on a Wind Turbine Wake: 3D Effects and Bluff Body Vortex Shedding*, Wind Energy 2006, **9**:219-236

[31] B. Sanderse, *Aerodynamics of wind turbine wakes*, ECN

[32] J.F Ainslie, *Calculating the flow field in the wake of wind turbines*, Journal of Wind Engineering and Industrial Aerodynamics 1988, **27**:213-224

Appendix A

Calibration curves

A.1 Calibration of the torque

The torque and thrust transducers were calibrated using weight elements with known masses. The sensors are known to respond linearly to the forces acting on the turbine. First the calibration measurements were done with increasing masses, and then followed by decreasing the mass back to 0. This was done to decrease the effect of hysteresis [7]. Linear regression was used to find the calibration curve.

The sensitivity of the torque transducer was calibrated prior to the tests by using calibrated weights applied to the tip of one of the blades when this was locked in a horizontal position. The results for the calibration of the torque on the wind turbine are shown in figure A.1. The calibration constant is K=$Moment/\Delta V = -0,2088[Nm]/[V]$, and the calibration was done with no gain (Gain=1). The equation for the torque on the wind turbine then becomes:

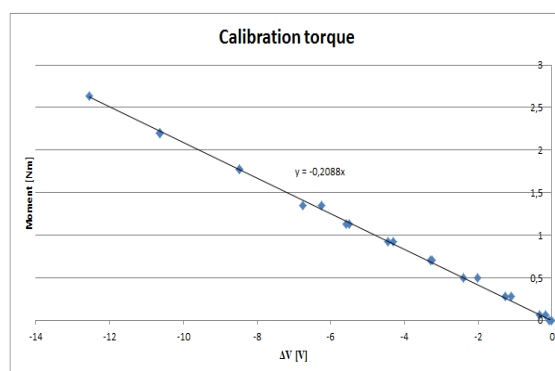$$Q = -0,2088(V - V_{offset}) \tag{A.1}$$

Figure A.1: Calibration curve for the torque on the wind turbine.

A.2 Calibration of the thrust force

The calibration of the thrust force on the wind turbine was done by measuring the voltage output for weight elements with known masses connected to the force plate. First the mass was increased in steps from 0 g to about 9500 g, and then decreased with the same steps back to 0 g. The force F=mg has a linear relationship with the voltage output, but the voltage output often differs a little bit when the mass is decreasing than if it is increasing. This is due to a factor which is called hysteresis [7], and may cause a small error to the calibration constants. The calibration plot is shown in figure A.2, and the calibration constant for the thrust is K=$Force/\Delta V = 8,2692[N]/[V]$. The measurements for the thrust force was done with a gain of 4 and the equation is:

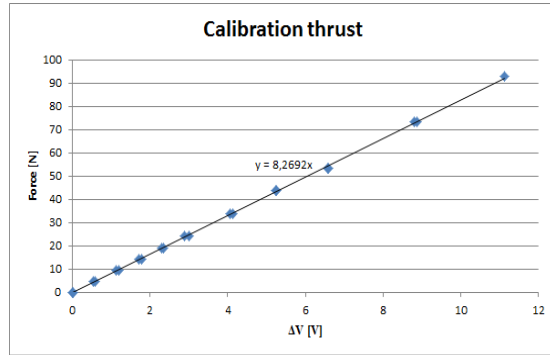$$T = 8,2692(V - V_{offset}) \tag{A.2}$$

Figure A.2: Calibration curve for the thrust force on the wind turbine.

A.3 Calibration of pressure transducers

The pressure transducers for the contraction of the wind tunnel and the pitot tube were calibrated by using a manometer to find the pressure differences for different wind speeds. The pressure difference versus the voltage output was plotted to find the calibration constants, which is the slope of the linearisation of the curve.

A pitot tube is an instrument to measure the mean velocity in a fluid. The tube is oriented parallel to the flow, and has two pressure-sensor locations, one for the total pressure and one for the static pressure. The total pressure is the sum of the static pressure and the dynamic pressure, and the pressure difference can be used to calculate the velocity:

$$p_{tot} = p_s + \frac{1}{2}\rho V^2 \tag{A.3}$$

$$V = \sqrt{\frac{2(p_{tot} - p_s)}{\rho}} \tag{A.4}$$

The pressure difference is read from a manometer during the calibration, and for this experiment, a calibration constant of K=15,438 Pa/V with a gain of 4 was calculated, which is shown in figure A.3. The pitot tube was also used in the calibration of the hot wire.
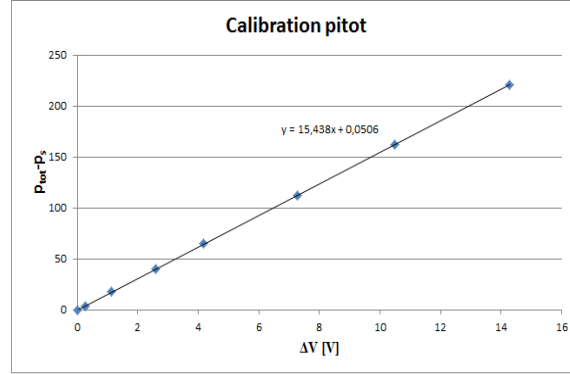

Figure A.3: Calibration curve for the pitot pressure transducer.

The wind tunnel has a contraction upwind of the wind turbines with the area differences $\frac{A1}{A2} = 4,36$, where the subscript 1 and 2 denotes before and after the contraction, respectively. There is a pressure transducer that measures the pressure difference before and after the contraction, and the calibration resulted in a calibration constant of K=12,81 Pa/V with a gain of 5. The calibration was done by reading the pressure difference $p_1 - p_2$, before and after the contraction, from a manometer for different wind speeds. Then linear regression was used to find the slope of the curve, and the curve is shown in figure A.4.
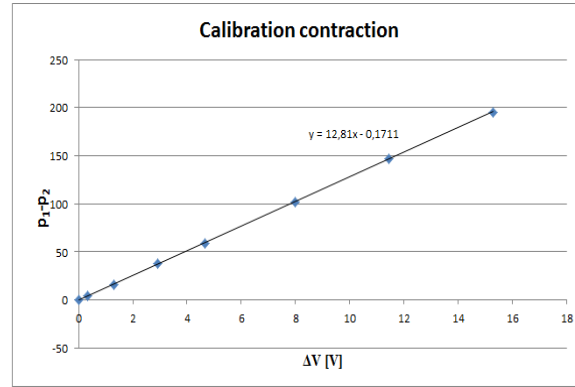

Figure A.4: Calibration curve for the contraction pressure difference.

The velocity after the contraction, V_2, was calculated from Bernoulli's equation and the continuity equation:

$$\frac{Q}{A_2} = V_2 = \sqrt{\frac{2}{\rho} \frac{(p_1 - p_2)}{(1 - (\frac{A_2}{A_1})^2)}} \tag{A.5}$$

A constant C is multiplied with V_2 to compensate for non-ideal effects, to find the real reference wind speed: $U_{ref} = C \cdot V_2$. This factor was found by the use of a pitot tube

59

placed where the centre of the rotor was supposed to be, and comparing this velocity with V_2 from equation A.5. This resulted in the correction factors $C = \frac{1}{0,984}$ without the grid in the tunnel and $C = \frac{1}{1,1538}$ with the grid in the tunnel.

A.4   Calibration of the hot wire

The calibration of the hot wire is done by using a pitot tube to measure the mean velocity, and then find the correlation between the voltage output from the hot wire and the mean wind speed. The hot wire is most sensitive at low wind speeds, but the uncertainty is also highest in this area. The calibration curve for a hot wire is non-linear, and a fourth-order polynomial fits relatively well to the curve. An example of one of the hot wire calibration curves is shown in figure A.5.
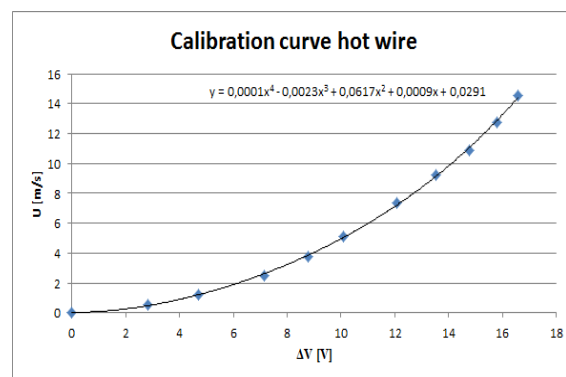

Figure A.5: Calibration curve for the hot wire.

Appendix B

Experimental results for performance characteristics

B.1 Results without grid

Temperature[℃]	Ω	U_{ref}	Power[W]	Torque[Nm]	Thrust[N]
23,79	23,67	11,26	6,53	0,28	10,32
24,11	44,61	11,22	18,83	0,42	13,86
24,34	67,75	11,16	46,71	0,69	18,72
24,51	88,70	11,12	140,03	1,58	24,86
24,77	111,11	11,00	218,06	1,96	33,08
24,87	133,41	11,03	233,44	1,75	38,24
25,00	151,95	11,02	230,36	1,52	41,37
25,09	173,42	11,00	215,67	1,24	44,37
25,14	195,30	10,99	185,31	0,95	46,80
25,28	216,98	10,98	141,45	0,65	48,65
25,41	238,97	11,00	93,86	0,39	50,92
25,50	258,66	10,95	27,38	0,11	52,38

Table B.1: Results from lab experiment for performance characteristics without grid.

B.2 Results with grid

Temperature[°C]	Ω	U_{ref}	Power[W]	Torque[Nm]	Thrust[N]
24,96	22,62	10,51	4,91	0,22	9,64
25,30	44,72	10,49	16,80	0,38	13,47
25,49	67,75	10,47	47,40	0,70	18,12
25,73	89,43	10,43	140,13	1,57	24,79
25,83	109,64	10,41	182,30	1,66	31,32
25,94	132,37	10,38	189,27	1,43	35,80
26,18	154,88	10,37	179,91	1,16	39,04
26,25	175,09	10,37	162,87	0,93	41,65
26,43	197,50	10,35	129,86	0,66	43,96
26,49	220,02	10,33	82,69	0,38	45,63
26,55	240,75	10,34	30,13	0,13	47,29
26,65	261,38	10,33	-34,21	-0,13	48,45

Table B.2: Results from lab experiment for performance characteristics with grid.

Appendix C

Wing profile

C.1   NREL s826

The wing profile used for the turbine blades on the wind turbine in lab is NREL s826. The geometry is shown in figure C.1. The chord length and twist angle distribution along the blade are shown in figure C.3 and C.2.
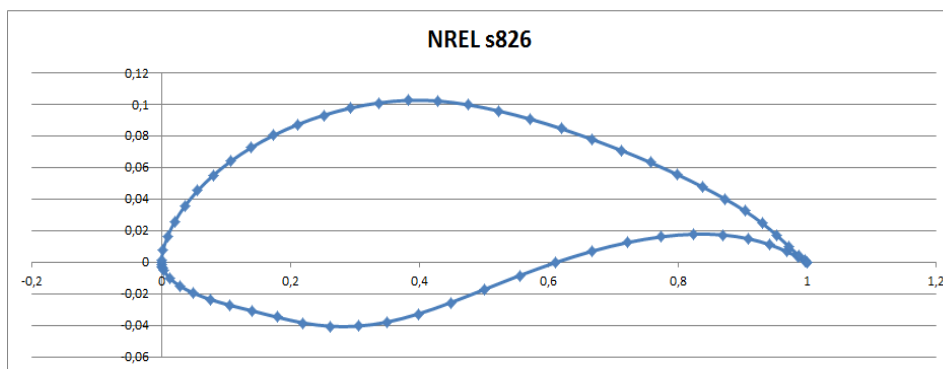

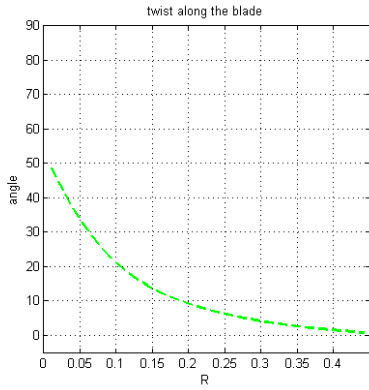Figure C.1: Geometry of wing profile NREL s826
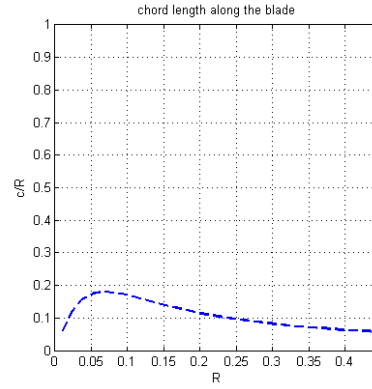
Figure C.2: Twist angle along the blade.

Figure C.3: Chord length along the blade.

C.2 Lift and drag coefficients

The lift and drag coefficients for the NREL s826 wind profile are shown in figure C.4 and C.5 respectively. The design condition for the blade is an angle of attack of 7 °and a tip speed ratio of 5.
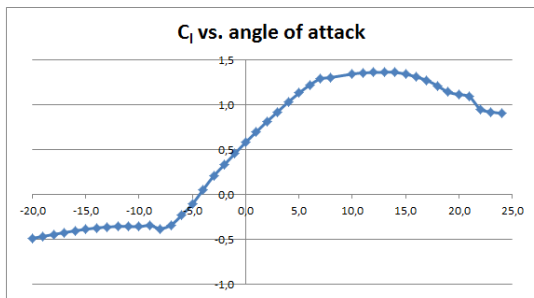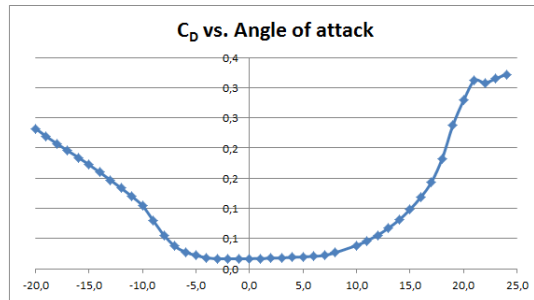

Figure C.4: Lift coefficients versus angle of attack.

Figure C.5: Drag coefficients versus angle of attack.

Appendix D

Error analysis of power coefficient values

During the lab experiment to find the performance characteristics for the wind turbine, both the mean values and the RMS (Root Mean Square) values were measured and logged. The RMS value is the same as the standard deviation for the samples, and this value was logged for the torque, the thrust, the rotational speeds, the contraction pressure difference and the temperature. The mean and RMS values can be used to calculate the random errors of the lab experiment

The total uncertainty of the mean values from the lab experiment is due to a combination of systematic errors and random errors [7]. Systematic errors, also called the bias, are consistent and repeatable, for example calibration errors, loading errors and spatial errors. This error is the difference between the true value and the average value of the readings. An instrument with low bias is therefore accurate. Random errors, also called precision or probabilistic errors, arise from random fluctuations of the instruments. An instrument with low random error is precise. A schematic of the difference between the systematic error and the random error is shown in figure D.1.
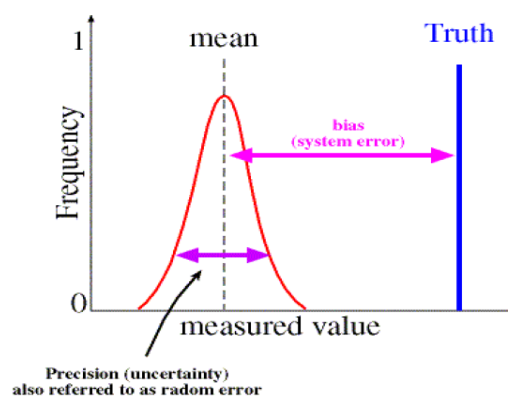

Figure D.1: Schematic showing difference of systematic and random error.

To estimate the total uncertainty of a mean of a population, $\omega_{\bar{x}}$, based on the bias B and the probabilistic error P, the following equation is used:

$$\omega_{\bar{x}} = \sqrt{B_{\bar{x}}^2 + P_{\bar{x}}^2} \qquad (D.1)$$

The systematic errors in this Master Thesis are expected to be the maximum deviations between the measured points and the fitting curve of the calibrations. The systematic error is therefore only known for the instruments that were calibrated, hence the torque, the thrust and the pressure transducer for the contraction. For the other instruments where the systematic error is unknown, the total error is assumed to only consist of the random error.

The random errors in this Master Thesis are calculated with a confidence interval of 95 %, and the t-distribution is used to calculate this. If S_x is the standard deviation of the mean value of a population, n is the number of samples and is bigger than 30, the random uncertainty for the mean of a population is given by:

$$P_{\bar{x}} = \pm t \frac{S_x}{\sqrt{n}} \qquad (D.2)$$

The variable t depends on the size of the confidence interval, and for a confidence interval of 95 % and n=6000, a value of 2 can be used for t. S_x is in this case the RMS values from the samples. A more detailed description of different errors and uncertainty estimations can be found in [7].

If a result R is a function of variables x_i with different errors, $R = f(x_1, x_2, ..., x_n)$, an equation known as *The root of the sum of the squared* (RSS) is used to combine the errors and find the total error for R:

$$\omega_R = (\sum_{i=1}^{n} [\omega_{x_i} \frac{\delta R}{\delta x_i}]^2)^{1/2} \qquad (D.3)$$

where ω_{x_i} is the result from equation D.1 for each variable.

To find the error for the power coefficient, first equation 2.15 needs to be inspected. The power of the turbine is calculated from it's torque multiplied with it's rotational speed: $P = Q \cdot \Omega$. The density is dependent of the temperature and the atmospheric pressure through the ideal gas law, while the reference velocity is calculated as shown in appendix A.3. The equation for C_p becomes:

$$C_p = \frac{\sqrt{p_{atm}} \cdot (1 - (A_2/A_1)^2)^{3/2}}{\sqrt{2 \cdot R_{air}} \cdot A_{rotor} \cdot C^3} \cdot \frac{Q \cdot \Omega}{\sqrt{T} \cdot (p_1 - p_2)^{3/2}.} \qquad (D.4)$$

R_{air} is here the air gas constant, Ω is the rotational speed and T is the temperature in Kelvin.

The systematic error for the torque, Q, is 0,07381 Nm, while it is 7,2 Pa for the pressure transducer for the contraction, $p_1 - p_2$. The systematic error for the other instruments were unknown. The random errors were calculated from equation D.2 for Q, T and $(p_1 - p_2)$. The standard deviation for the other parameters were unknown. Then all the

errors were combined by the use of equation D.1 and D.3. The result for the peak power coefficient values included 95 % confidence interval error bars is shown in figure D.2. The total uncertainty for the peak power coefficient without grid is approximately 2 %, but the real value is probably a little higher since some of the systematic errors and standard deviations were unknown and therefore neglected. The mean peak power coefficient of 0,461 can therefore vary between 0,456 and 0,466 with a confidence interval of 95 % from these error calculations. The Cp curve without free stream turbulence including the 95 % error bars are shown in figure D.2.

The results from the uncertainty calculations with grid turbulence are very similar, and the total uncertainty for the peak power coefficient of 0,45 is approximately 1,7 %. The Cp curve with free stream turbulence including the 95 % error bars are shown in figure D.3.
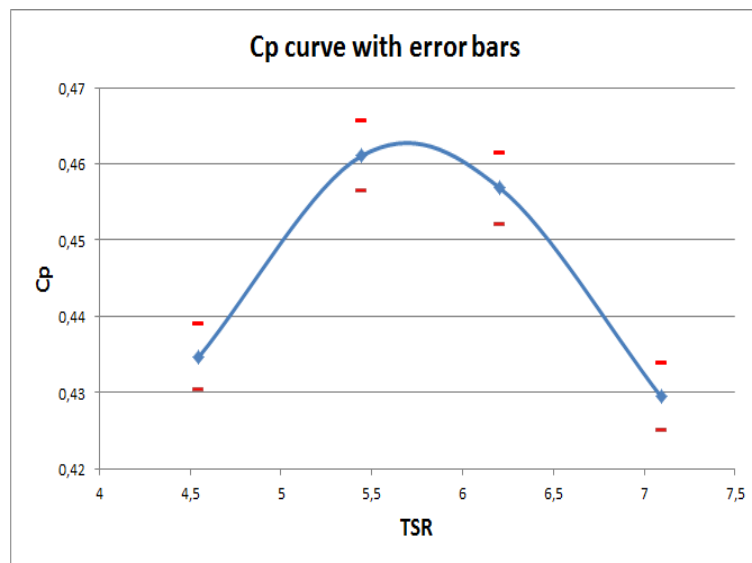

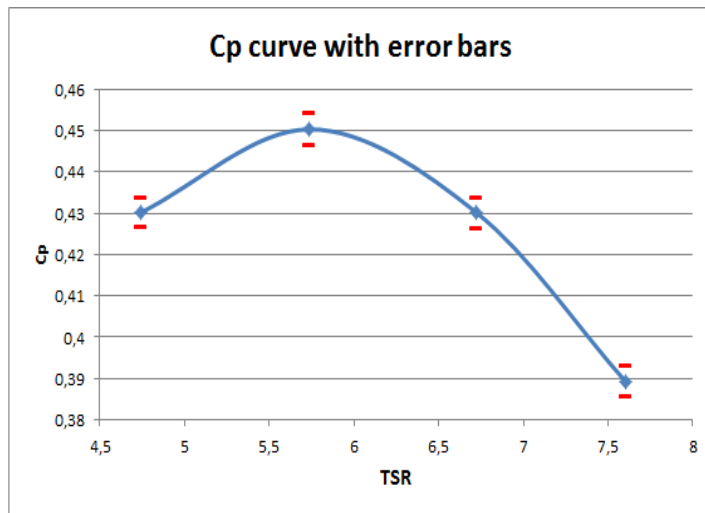Figure D.2: C_P curve without grid including error bars.

Figure D.3: C_P curve with grid including error bars.

Appendix E

Risk assessment of the lab experiment

The facilities in the lab and the lab experiment in the wind tunnel in the Fluid Mechanics building at NTNU has gone through risk assessments before, and is considered as a safe environment. To get access to the lab in the Fluid Mechanics building, I took the required e-learning course and had a guided safety tour in the lab in advance of the lab experiments.